



HAL
open science

Textural signatures of sediment supply in gravel-bed rivers: Revisiting the armour ratio

Daniel Vázquez-Tarrío, Hervé Piégay, Rosana Menéndez-Duarte

► To cite this version:

Daniel Vázquez-Tarrío, Hervé Piégay, Rosana Menéndez-Duarte. Textural signatures of sediment supply in gravel-bed rivers: Revisiting the armour ratio. *Earth-Science Reviews*, 2020, 207, pp.103211. 10.1016/j.earscirev.2020.103211 . hal-03025266

HAL Id: hal-03025266

<https://hal.science/hal-03025266>

Submitted on 22 Dec 2020

HAL is a multi-disciplinary open access archive for the deposit and dissemination of scientific research documents, whether they are published or not. The documents may come from teaching and research institutions in France or abroad, or from public or private research centers.

L'archive ouverte pluridisciplinaire **HAL**, est destinée au dépôt et à la diffusion de documents scientifiques de niveau recherche, publiés ou non, émanant des établissements d'enseignement et de recherche français ou étrangers, des laboratoires publics ou privés.

Textural signatures of sediment supply in gravel-bed rivers: revisiting the armour ratio

Daniel Vázquez-Tarrío^{1,2}, Hervé Piegay³ and Rosana Menéndez-Duarte^{1,2}

¹ Department of Geology, University of Oviedo, c\ Jesús Arias de Velasco, s/n 33005 Oviedo, Spain. danielvazqueztarrio@gmail.com

² INDUROT, University of Oviedo, Campus de Mieres, s/n 33600 Mieres, Spain

³ University of Lyon, CNRS UMR 5600 EVS, Site ENS, F-69342 Lyon, France

Abstract:

The surface of the streambed in gravel-bed rivers is commonly coarser than the underlying bed material. This surface coarsening, or ‘armouring’, is usually described by means of the ratio between surface and subsurface grain-size metrics (the ‘armour ratio’). Such surface coarsening is typical of river reaches that are degrading due to a deficit in sediment supply (e.g. gravel-bed reaches below dams or lakes), but non-degrading gravel-bed streams may also exhibit some degree of armouring in relation to specific hydrological patterns. For instance, selective transport during the recession limbs of long lasting floods may coarsen the bed more significantly than flash floods. Consequently, regional differences in bed coarsening should exist, reflecting in turn the variability in sediment and water regimes. In this paper, we explore the trends linking armour ratios to sediment supply, taking into account the differences in hydrological context. We based our analysis on a large data set of bedload and grain size measurements from 49 natural gravel-bed streams and four flume experiments compiled from the scientific literature. Our main outcome documents how the balances between sediment yields and transport capacities have a quantifiable reflection on the armour ratios measured in the field: we report strong and statistically significant correlations between bedload fluxes and surface grain-size, and an asymptotic rise in armour ratios with the decline of sediment supply. Hydrological controls are also observed, but they are small compared to the signal related to sediment supply. Additionally, the trends observed in the field data are comparable to those previously documented in flume experiments with varying sediment feed. In this regard, different kinds of bedforms and particle arrangements have been commonly described with progressive reductions in sediment inputs and the subsequent coarsening of the streambed. Hence, armour ratios serve as a proxy for the general organization of the streambed of gravel-bed streams, and our results quantify this streambed adjustment to the dominant sediment supply regime.

Keywords: Gravel-bed rivers, Armour ratio, Sediment supply, Bedload

1. Introduction

A longstanding idea in fluvial geomorphology is that balances between sediment transport capacities, water discharge and sediment supply influence channel geometry (Parker et al., 2007; Parker, 2008), bed slope (e.g. Lane, 1955; Borland, 1960; Wilcock et al., 2009), streambed texture (Dietrich et al., 1989; Nelson et al., 2009; Venditti et al., 2017) and planform morphology (Church, 2006). Short-term fluctuations in sediment supply (e.g. hillslope processes, bank erosion, fine release from the bed after large floods) lead to local and temporary adjustments in streambed texture (e.g. Church et al., 1998; Clayton and Pitlick, 2008; Turowski et al., 2011) and channel morphology (Hassan and Zimmerman, 2012). In the long term, the balances between sediment and water yields seem to exert a conspicuous control on dominant channel styles (Montgomery and Buffington, 1997; Buffington, 2012) and river metamorphosis (Métivier and Barrier, 2012).

Seminal flume experiments by Dietrich et al. (1989), and early field observations (e.g. Gessler, 1967; Willets et al., 1988), reported how reductions in sediment supply tend to promote active channel narrowing, surface coarsening, bedload fining and transport rate decrease in gravel-bed rivers. Coarsening and fine sediment depletion in the riverbed is driven by a combination of winnowing during low flows (Gomez, 1983, 1993, 1994), infiltration of fine sediment (Marion and Fraccarollo, 1997; Curran and Waters, 2014; Berni et al., 2018) and kinematic sorting (Wilcock, 2001; Bacchi et al., 2014; Ferdowski et al., 2017) during bed load transport. Substantial subsequent work documents the influence of sediment inputs on the spatial and vertical patterns of grain size sorting (Nelson et al., 2009; 2010), the development of particle arrangements (e.g. Church et al., 1998; Venditti et al., 2017) and overall streambed mobility (Richards and Clifford, 1991; Pfeiffer and Finnegan, 2018).

According to all of the above, surface grain-size responds to decreases in bedload through the expansion of coarse fixed patches (Nelson et al., 2009; Yager et al., 2015), resulting in a general coarsening of the streambed (Dietrich et al., 1989). Hence, the degree of the latter may provide an idea of the dominant sediment supply conditions of a given river reach (Dietrich et al., 1989; Sklar et al., 2009; Venditti et al., 2017). For this reason, fluvial geomorphologists have often used

60
61
62 29 the field observation of surface coarsening as a way to characterize streambed mobility and/or to
63
64 30 diagnose the magnitude of bed degradation below dams, for example (see Rollet et al. 2013;
65
66 31 Vázquez-Tarrio et al. 2019). However, disparities in the patterns of sediment supply variability
67
68 32 (e.g. at the annual, seasonal, intra-flood scale) between different hydrological contexts complicate
69
70 33 the interpretation of surface coarsening measured in the field and its application to river diagnosis.
71
72 34 For instance, rivers experiencing long-lasting and sustained floods tend to exhaust fine sediment
73
74 35 from the riverbed, which in turn enhances the degree of coarsening compared to the situation
75
76 36 expected in streams with comparable sediment supplies, but submitted to flash floods (Laronne
77
78 37 et al., 1994; Hassan et al. 2006). The hydrological regime is then a source of variability in the
79
80 38 degree of surface coarsening that overlaps the signal related to the dominant sediment supply
81
82 39 conditions. Moreover, sediment supply is difficult to quantify due to inherent complexities in
83
84 40 bedload measurement (Pitlick et al., 2012); therefore, the field assessment of streambed response
85
86 41 to sediment supply fluctuations is not easy.

87
88 42 In this paper, we build on these ideas in order to quantify the relative weight of sediment supply
89
90 43 versus hydrological controls in governing surface armouring. To accomplish this, we based our
91
92 44 analysis on a large compilation of grain-size measurements and bedload discharge information
93
94 45 extracted from the scientific literature for 49 natural gravel-bed rivers and four flume experiments.
95
96 46 We structured this analysis in two steps. First, we performed a wide review of the compiled grain-
97
98 47 size data, from which metrics adequate for exploring the links between bed texture and sediment
99
100 48 supply were identified. Then, we performed a meta-analysis of the compiled data (based on the
101
102 49 metrics introduced in the review) in order to highlight the main trends in armour ratios, and their
103
104 50 covariation with channel hydraulics and bedload fluxes. Understanding the linkages between
105
106 51 streambed texture and sediment transport regime is a key question in fluvial geomorphology, river
107
108 52 ecology, civil engineering and river restoration (Pfeiffer et al., 2017). Consequently, our analysis
109
110 53 may have interesting implications for near-future research on gravel-bed rivers.
111
112
113
114
115
116
117
118

119
120
121 **54 2. Compiled data**
122

123 55 The dataset used in the present paper consists of grain-size and bedload measurements collected
124
125 56 at 49 river sites (summarized in Table 1). An important amount of the compiled data derives from
126
127 57 the extensive campaign of sediment transport measurements carried out on Idaho, Nevada (King
128
129 58 et al., 2004), Colorado and Wyoming rivers (Ryan et al., 2002; 2005), which probably represents
130
131 59 some of the best available datasets on bedload in gravel-bed rivers to date. These data have
132
133 60 previously been presented and analysed in several papers (Ryan et al., 2002; 2005; King et al.,
134
135 61 2004; Barry et al., 2004; Mueller et al., 2005; Muskatirovic, 2008; Pitlick et al., 2008). The
136
137 62 remaining data come from comparable measurements in other gravel-bed streams (Milhous, 1973;
138
139 63 Emmet and Seitz, 1974; Seitz, 1977; Jones and Seitz, 1980; Reid and Frostick, 1986; Lisle, 1986;
140
141 64 1989; Williams and Rosgen, 1986; Gomez, 1988; Kuhle, 1992; Lisle and Madej, 1992; Andrews,
142
143 65 1994; Reid et al., 1995; Madej and Ozaki, 1996; McLean et al., 1999; Almedej, 2002; Church and
144
145 66 Hassan, 2002; Wilcock and Kenworthy, 2002; Erwin et al., 2011; Mueller and Pitlick, 2014).
146
147 67 Grain sizes (surface and substrate/subsurface) for each selected river were obtained from the
148
149 68 graphical reading of grain-size curves extracted from the corresponding papers. When bed
150
151 69 material was sampled at several locations or moments in the same river, we averaged the results
152
153 70 to obtain a characteristic grain-size measure for each case study. Stream discharge information is
154
155 71 available for 44 of the 49 selected case studies, together with width-averaged data on the main
156
157 72 flow characteristics (velocity, active width). Using this information, we computed bed shear stress
158
159 73 based on Rickenmann and Recking's (2011) fit to Ferguson's (2007) friction law (for more details
160
161 74 see the supplementary files). We also compiled, for each case study, values for the representative
162
163 75 channel-forming or dominant discharge (Table 2), which were derived from the information
164
165 76 provided in the original papers about the bankfull discharge (in single-thread channels) or the ~1
166
167 77 to 2-year return period discharge (in multi-thread channels) (Table 2). Information on bedload
168
169 78 discharges was also available (Table 1); in this regard, we acknowledge the great work of data
170
171 79 compilation carried out by Recking (2010; 2013), who provided bedload information for these
172
173 80 field sites as supporting files (ibid).
174
175
176
177

178
179
180
181
182
183
184
185
186
187
188
189
190
191
192
193
194
195
196
197
198
199
200
201
202
203
204
205
206
207
208
209
210
211
212
213
214
215
216
217
218

River/Reach	Source	Channel style	Slope	Surface D ₈₄ (mm)	Subsurface D ₈₄ (mm)	GSD measuring method		Flow width (m)	Flow depth (m)	Q (m ³ /s)	Q _b (g/s·m)	N	Sediment sampling method
						Surface	Subsurface						
Big Wood River	<i>King et al. (2004)</i>	Plane-bed	0.091	250	101	Pebble count and core sampling	Core sampling	12.8	0.4-1.1	6.0-30.9	0.0-336.4	100	HS 7.62 or 15.2 cm (0.25 mm mesh)
Blackmare Creek	<i>King et al. (2004)</i>	Plane-bed	0.03	220	97	Pebble count and core sampling	Core sampling	4.94-11.89	0.1-0.5	0.3-4.7	0.0-6.8	88	HS 7.62 or 15.2 cm (0.25 mm mesh)
Boise river	<i>King et al. (2004)</i>	Riffle and pool	0.0038	141	86	Pebble count	Core sampling	52.4-61.0	0.6-2.1	33.7-291.7	0.4-633.5	82	HS 7.62 or 15.2 cm (0.25 mm mesh)
Borgne d'Arolla	<i>Gomez (1988)</i>	Step-Pool	0.03	19	12	Contact sampling technique	10 kg-volumetric sampling	0.3-2.2	0.0-0.1	0.0-0.3	56.2-837.0	31	HS (7.6 cm), 0.5 mm mesh
Chulitnana River	<i>Williams and Rossen (1989)</i>	Braided	0.0008	52	184	Pebble count (?)	Dredge sampling	98.5-309.0	1.7-3.6	212.0-7104.0	213.0-2590.0	43	HS (7.62 cm)
Clearwater River	<i>Jones and Seiz (1980)</i>	Riffle and pool	0.00037	70	70	Pebble count	Sieve analysis of dug material	125.0-149.0	3.4-46.3	288.0-3511.0	0.1-284.0	78	HS (7.6 and 15 cm)
Dollar Creek	<i>King et al. (2004)</i>	Plane-bed	0.0146	145	83	Pebble count and core sampling	Core sampling	7.0-11.9	0.2-0.5	0.4-6.4	0.0-9.7	85	HS 7.62 or 15.2 cm (0.25 mm mesh)
East Fork San Juan	<i>Ryan et al. (2005)</i>	Braided	0.008	112	52	Pebble count	Barrel method	15.0-17.2	0.3-0.5	2.8-13.8		77	Wadable version of Elwha sampler, 102 × 203 mm
East Saint-Louis Creek	<i>Ryan et al. (2002)</i>	Step-Pool	0.058	142	23	Pebble count	Barrel method	2.8-3.0	0.1-0.4	0.1-1.24	0.0-21.2	109	HS (7.6 cm)
Fool Creek	<i>Ryan et al. (2002)</i>	Plane-bed	0.053	100	59	Pebble count	Barrel method	1.7-2.1	0.1-0.2	0.0-0.5	0.0-14.7	95	HS (7.6 cm)

219
220
221
222
223
224
225
226
227
228
229
230
231
232
233
234
235
236
237
238
239
240
241
242
243
244
245
246
247
248
249
250
251
252
253
254
255
256
257
258
259

River/Reach	Source	Channel style	Slope	Surface D ₈₄ (mm)	Subsurface D ₈₄ (mm)	GSD measuring method	Flow width (m)	Flow depth (m)	Q (m ³ /s)	Q _b (g/s·m)	N	Sediment sampling method
	<i>McLean et al. (1999); Ferguson and Church (2009)</i>											Basket sampler (610 × 255 mm) for high flows and half-size VuV sampler (225 × 115 mm) for lower flows
Fraser River		Riffle and pool	0.00046	70	68	Pebble count	510	-	1085-11445	0.3-486.3	76	
Goodwin Creek	<i>Kuhnle (1992); Almedeij (2002)</i>	Riffle and pool	0.0021	30	30	Pebble count	11.1-14.6	0.4-1.2	1.4-21.6	0.2-2980.0	357	HS (58 cm2 with trapezoidal shape), 0.25mm net mesh
Harris Creek	<i>Church and Hassan (2002)</i>	Riffle and pool	0.013	100	55	Pebble count (grid-by-number)	15	-	4.2-18.4	0.0-4.3	22	Sediment trap
Jacoby	<i>Lisle (1986); Lisle (1989); Almedeij (2002); Wilcock and Kenworthy (2002)</i>	Riffle and pool	0.0063	95	81	Pebble count	17.2	-	0.6-18.51	0.0-413.0	100	HS (4.4 cm)
Johns Creek	<i>King et al. (2004)</i>	Step-Pool	0.0207	558	63	Pebble count	8.2-14.6	0.3-1.2	1.0-34.3	0.0-10.7	46	HS 7.62 or 15.2 cm (0.25 mm mesh)
Little Buckhorn Creek	<i>King et al. (2004)</i>	Step-Pool	0.0509	340	94	Pebble count and core sampling	1.4-4.6	0.1-0.7	0.1-0.7	0.0-18.5	78	HS 7.62 or 15.2 cm (0.25 mm mesh)

260
261
262
263
264
265
266
267
268
269
270
271
272
273
274
275
276
277
278
279
280
281
282
283
284
285
286
287
288
289
290
291
292
293
294
295
296
297
298
299
300

River/Reach	Source	Channel style	Slope	Surface D ₈₄ (mm)	Subsurface D ₈₄ (mm)	GSD measuring method		Flow width (m)	Flow depth (m)	Q (m ³ /s)	Q _b (g/s·m)	N	Sediment sampling method
						Surface	Subsurface						
Little Granite Creek	<i>Ryan et al. (2002)</i>	Plane-bed	0.019	220	41	Pebble count	Barrel method	6.5-11.2	-	0.7-11.6	0.0-128.0	123	HS 7.62 cm
Little Slate	<i>King et al. (2004)</i>	Plane-bed	0.0268	380	141	Pebble count and core sampling	Core sampling	6.7-13.4	0.3-1.0	0.5-18.3	0.0-10.3	157	HS 7.62 or 15.2 cm (0.25 mm mesh)
Lochsa Creek	<i>King et al. (2004)</i>	Plane-bed	0.0023	245	123	Pebble count and core sampling	Core sampling	67.1-83.0	1.8-3.1	110.7-758.9	0.0-48.3	72	HS 7.62 or 15.2 cm (0.25 mm mesh))
Lolo Creek	<i>King et al. (2004)</i>	Plane-bed	0.0097	140	68	Pebble count and core sampling	Core sampling	10.7-16.0	0.3-1.5	1.8-23.0	0.0-13.4	89	HS 7.62 or 15.2 cm (0.25 mm mesh)
Middle Fork	<i>King et al. (2004)</i>	Plane-bed	0.0041	288	140	Pebble count and core sampling	Core sampling	42.7-67.1	1.2-2.01	83.5-433.2	0.1-727.7	64	HS 7.62 or 15.2 cm (0.25 mm mesh)
Middle Fork Piedra River	<i>King et al. (2004)</i>	Riffle and pool	0.011	210	43.3	Pebble count and core sampling	Core sampling	11.4-13.8	0.2-0.5	1-11.0	0.0-216.6	86	HS 7.62 or 15.2 cm (0.25 mm mesh)
Nahal Yatir	<i>Reid et al. (1995)</i>	Riffle and pool	0.0088	13	34	Removing clasts from spray-painted stripes and laboratory sieving	Bulk volume sampling	3.5	0.1-0.6	0.3-0.5	200.0-7050.0	74	Sediment trap
North Fork Clearwater	<i>King et al. (2004)</i>	Plane-bed	0.0005	270	104	Pebble count and core sampling	Core sampling	9.1-93.6	1.7-34.1	100.8-974.1	0.0-732.2	72	HS 7.62 or 15.2 cm (0.25 mm mesh)
Oak Creek	<i>Milhous (1973)</i>	Plane-bed	0.0083	80	52	Pebble count and bottom samplers	Bulk volume sampling	3.7	-	0.0-3.4	0.0-111.0	119	Sediment trap, vortex tube

301
302
303
304
305
306
307
308
309
310
311
312
313
314
315
316
317
318
319
320
321
322
323
324
325
326
327
328
329
330
331
332
333
334
335
336
337
338
339
340
341

River/Reach	Source	Channel style	Slope	Surface D ₈₄ (mm)	Subsurface D ₈₄ (mm)	GSD measuring method		Flow width (m)	Flow depth (m)	Q (m ³ /s)	Q _b (g/s·m)	N	Sediment sampling method
						Surface	Subsurface						
Pacific creek	<i>Erwin et al. (2011)</i>	Braided	0.0035	45	28	Pebble count	Bulk volume sampling	-	-	-	-	-	-
Rapid River	<i>King et al. (2004)</i>	Plane-bed	0.0108	170	101	Pebble count	Core sampling	11.4-18.6	0.2-0.9	0.9-36.8	0.0-294.3	190	HS 7.62 or 15.2 cm (0.25 mm mesh)
Redwood Creek	<i>Lisle and Madej (1992); Madej and Ozaki (1996)</i>	Riffle and pool	0.0014	18	20	Pebble count	Bulk volume sampling	11.7-70	-	1.8-569	8.1-5067.8	221	HS sampler (7.6 cm)
Saint-Louis Creek	<i>Ryan et al. (2002; 2005)</i>	Plane-bed	0.0110-0.0450	162-543	33-78	Pebble count	Barrel method	5.2-10.3	0.1-0.4	0.4-7.2	0.0-65.7	813	HS (7.6 cm)
Sagehen Creek	<i>Andrews (1994)</i>	Riffle and pool	0.0102	104	96	Pebble count	Bulk volume sampling	2.6	0.3-1.6	1.0-3.1	0.5-34.9	55	HS (15 cm)
Salmon River below Yankee	<i>King et al. (2004)</i>	Plane-bed	0.0034	276	99	Pebble count and core sampling	Core sampling	30.5-38.4	1.2-1.9	38.5-143.6	0.0-98.8	60	HS 7.62 or 15.2 cm (0.25 mm mesh)
Salmon River near Obsidian	<i>King et al. (2004)</i>	Plane-bed	0.0066	128	84	Pebble count and core sampling	Core sampling	12.0-14.3	0.7-0.9	7.5-21.0	0.7-103.4	50	HS 7.62 or 15.2 cm (0.25 mm mesh)
Salmon River near Shoup	<i>King et al. (2004)</i>	Plane-bed	0.0019	174	136	Pebble count and core sampling	Core sampling	46.5-99.5	1.7-2.7	108.4-540.8	1.0-536.1	60	HS 7.62 or 15.2 cm (0.25 mm mesh)
Selway River	<i>King et al. (2004)</i>	Plane-bed	0.0021	265	173	Pebble count and core sampling	Core sampling	82.3-97.8	1.4-2.8	134.8-1067.5	0.0-43.5	72	HS 7.62 or 15.2 cm (0.25 mm mesh)

342
343
344
345
346
347
348
349
350
351
352
353
354
355
356
357
358
359
360
361
362
363
364
365
366
367
368
369
370
371
372
373
374
375
376
377
378
379
380
381
382

River/Reach	Source	Channel style	Slope	Surface		Subsurface		GSD measuring method		Flow width (m)	Flow depth (m)	Q (m ³ /s)	Qb (g/s·m)	N	Sediment sampling method
				D ₈₄ (mm)	D ₈₄ (mm)	Surface	Subsurface	Surface	Subsurface						
Silver Creek	<i>Ryan et al. (2005)</i>	Plane-bed	0.0450	73	33			Pebble count	Barrel method	3.8-4.4	0.1-0.3	0.1-1.4	0.0-214.3	57	Wadable version of the Elwha sampler, 102 × 203 mm
Snake River	<i>Emmett and Seitz (1974); Seitz (1977)</i>	Riffle and pool	0.0009	115	54			Pebble count	Sieve analysis of dug material	155.4-204.2	3.3-6.2	779.0-4559.0	0.0-342.0	63	HS (7.6 and 15 cm)
Snake River below Jackson Lake	<i>Mueller and Pitlick (2014)</i>	Braided	0.0025	83	58			Pebble count	Bulk volume sampling	-	-	-	-	-	-
South Fork Payette	<i>King et al. (2004)</i>	Plane-bed	0.004	150	79			Pebble count and core sampling	Core sampling	43.6-51.8	0.4-1.7	20.4-180.9	-	-	HS 7.62 or 15.2 cm (0.25 mm mesh)
South Fork Red River	<i>King et al. (2004)</i>	Plane-bed	0.0146	150	161			Pebble count and core sampling	Core sampling	5.8-12.2	0.1-0.9	0.2-13.0	0.0-29.0	204	HS 7.62 or 15.2 cm (0.25 mm mesh)
Squaw Creek USGS	<i>King et al. (2004)</i>	Plane-bed	0.01	72	93			Pebble count and core sampling	Core sampling	3.3-14.1	0.2-0.4	0.1-7.6	0.0-23.0	92	HS 7.62 or 15.2 cm (0.25 mm mesh)
Sunlight Creek-4	<i>Mueller and Pitlick (2014)</i>	Braided	0.0075	94.6	43			Pebble count	Bulk volume sampling	-	-	-	-	-	-
Sunlight Creek-11	<i>Mueller and Pitlick (2014)</i>	Riffle and Pool	0.0091	79.2	55			Pebble count	Bulk volume sampling	-	-	-	-	-	-
Susitna River near Talkeetns	<i>Williams and Rosgen (1986)</i>	Braided	0.0015	96	260			Pebble count, bulk sampling (?)	Bulk sampling (?), dredge sampling	118.0-202.0	1.1-14.0	240.0-1310.0	0.9-156.0	39	HS (7.62 cm)

383
384
385
386
387
388
389
390
391
392
393
394
395
396
397
398
399
400
401
402
403
404
405
406
407
408
409
410
411
412
413
414
415
416
417
418
419
420
421
422
423

River/Reach	Source	Channel style	Slope	Surface D ₈₄ (mm)	Subsurface D ₈₄ (mm)	GSD measuring method		Flow width (m)	Flow depth (m)	Q (m ³ /s)	Q _b (g/s·m)	N	Sediment sampling method
						Surface	Subsurface						
Susitna River at Sunshine, Alaska	<i>Williams and Rosgen (1986)</i>	Braided	0.0017	88	163	Pebble count, bulk sampling (?)	Bulk sampling (?), dredge sampling	174.0-311.0	2.1-4.4	504.0-2800.0	33.7-1500.0	41	HS 7.62 cm
Talkeetna River near Talkeetna	<i>Williams and Rosgen (1986)</i>	Braided	0.00096	100	184	Bulk sampling (?)	Bulk sampling (?), dredge sampling	-	-	-	-	-	-
Thompson Creek	<i>King et al. (2004)</i>	Plane-bed	0.0153	110	132	Pebble count and core sampling	Core sampling	4.2-6.7	0.2-0.4	0.2-3.5	0.0-38.0	84	HS 7.62 or 15.2 cm (0.25 mm mesh)
Trapper Creek	<i>King et al. (2004)</i>	Step-Pool	0.0414	122	67	Pebble count and core sampling	Core sampling	3.5-6.4	0.1-0.6	0.1-3.8	0.0-31.3	166	HS 7.62 or 15.2 cm (0.25 mm mesh)
Turkey Brook	<i>Reid and Frostick (1986)</i>	Riffle and pool	0.0142	42	35	No information	No information	3	0.1-0.9	0.1-13.8	0.0-50.6	206	Pit traps
Valley Creek	<i>King et al. (2004)</i>	Plane-bed	0.0040	160	78	Pebble count and core sampling	Core sampling	17.7-42.3	0.4-1.3	3.9-40.2	0.0-56.8	192	HS 7.62 or 15.2 cm (0.25 mm mesh)

Table 1. Sources of field data and information compiled for this study. D_{84} : 84-th percentile of the grain-size distribution (GSD). Q : Flow discharges. Q_b : Bedload discharges. *HS*: Helley-Smith sampler. N : number of data.

424
425
426
427
428
429
430
431
432
433
434
435
436
437
438
439
440
441
442
443
444
445
446
447
448
449
450
451
452
453
454
455
456
457
458
459
460
461
462
463
464

River/Reach	Dominant discharge (m ³ /s)	Flow recurrence (years)	River/Reach	Dominant discharge (m ³ /s)	Flow recurrence (years)	River/Reach	Dominant discharge (m ³ /s)	Flow recurrence (years)	River/Reach	Dominant discharge (m ³ /s)	Flow recurrence (years)
Big Wood River	21.7	1.5	Harris creek	19.0	1	Oak Creek	3.4***	No info	Snake River below Jackson Lake	285**	1.5 - 2
Blackmare Creek	4.7*	1.1	Jacoby	19.6	No info	Rapid river	17.7*	1.4	South Fork Payette	86.4*	1.2
Boise river	167.1*	1.7	Johns creek	49.0*	3.4	Pacific creek	60.1	1.5 - 2	South Fork Red River	7.3*	1.5
Borgne d'Arolla	0.2*	<1	Little Buckhorn Creek	0.2	1	Redwood Creek	560*	2 - 5	Squaw Creek USGS	5.1*	1.6
Chulitnana River	1130**	2	Little Granite Creek	5.9*	1.5	Saint-Louis Creek	2.6 - 4.8*	1.5	Sunlight Creek-4	16.5**	1.5 - 2
Clearwater River	2662***	2.2 - 2.3	Little Slate	12.2*	1.4	Sagehen Creek	2	~1	Sunlight Creek-11	14**	1.5 - 2
Dollar Creek	6.4*	1.1	Lochsa Creek	446*	1.5	Salmon River below Yankee	118.1	1.5	Susitna River near Talkeetna	1270**	2
East Fork San Juan	15.7*	1.5	Lolo Creek	11.8*	1.2	Salmon River near Obsidian	12.5	1.5	Susitna River at Sunshine, Alaska	4020**	2
East Saint-Louis Creek	0.9*	1.5	Middle Fork	217	1.5	Salmon River near Shoup	320	1.5	Talkeetna River near Talkeetna	730**	2
Fool Creek	0.3*	1.5	Middle Fork Piedra River	10.1*	1.5	Selway River	651.3*	1.7	Thompson Creek	2.5*	1.6
Fraser River	8760	1	Nahal Yatir	7.9	No info	Silver Creek	1.3*	1.5	Trapper Creek	2.6*	1.9
Goodwin creek	10.6	No info	North Fork Clearwater	453.1*	1.5	Snake River	3426***	2.2 - 2.3	Turkey Brook	19.6	No info
									Valley Creek	24.1*	1.6

Table 2. Information on the dominant channel-forming discharge for the case study selected for the present meta-analysis. (*) Bankfull discharge. (**) Dominant discharge provided by Mueller and Pitlick (2014). (***) Reference discharge provided by Church and Rood (1983)

506
507
508 81 We grouped the data following three different criteria. We made an initial classification according
509
510 82 to dominant channel morphology, grouping the different case studies as riffle and pool, step-pool
511
512 83 and plane-bed channels (after Montgomery and Buffington, 1997). Due to its geomorphological
513
514 84 significance, we also defined a separate group for multi-thread rivers, in spite of the fact that each
515
516 85 single thread of a braided river commonly shows a riffle and pool or bar-pool morphology. We
517
518 86 also classified the different data according to the general sediment supply conditions at the
519
520 87 catchment scale (Table 3). Following Recking (2012), we defined three main groups of data: i.
521
522 88 low sediment supply, with channels draining highly vegetated watersheds and no clear active
523
524 89 sediment sources and/or alluvial material; ii. moderate sediment supply, with rivers located in
525
526 90 catchments in which significant bare land areas and/or sparse vegetation, and punctually
527
528 91 distributed active sediment sources, are observed; and iii. high sediment supply, with channels
529
530 92 well-coupled to landslides/slope deposits, or fed by strong bank erosion and/or bar-edge trimming
531
532 93 (e.g. channels with braided morphology). We based this classification on the scarce information
533
534 94 (study site description, photographs, etc.) provided by the original studies and our own inspection
535
536 95 of the rivers through Google Earth. Finally, we also grouped the compiled data according to
537
538 96 dominant flow regime, differentiating between: i. ‘rainfall-dominated’; ii. ‘snowmelt/rain-on-
539
540 97 snow-dominated’; iii. ‘snowmelt-dominated’; iv. ‘glacial-fed’ and v. ‘flash-flood dominated’
541
542 98 streams (Table 3).

543
544 99

Flume	Source	S	W (m)	L (m)	h (cm)	D _{50s} (mm)	Shields	Feed rate	r (h)
Tsukuba	<i>Nelson et al. (2009)</i>	0.0035-0.0052	7.5	0.3	10.2-11.3	3.7-4.9	0.049-0.086	1.7-17.4g/min·cm	6-7.5
Berkeley	<i>Nelson et al. (2009)</i>	0.0043-0.0055	28	0.9	21.8-22.8	10.1-11.8	0.045-0.061	0-23.3 g/min·cm	20.7-28.9
UBC	<i>Church et al. (1998)</i>	0.001-0.012	0.5/0.8	6/10	0.5-7.4	1.9-5.1	0.003-0.117	No feed	-
UBC	<i>Hassan and Church (200)</i>	0.006/0.007	0.8	10	0.1-6.7	2.4-4.5	-	1.2-0.644 kg/h	96

100 **Table 4.** Sources of flume data compiled for this study. *S*: Flume slope. *W*: Flume width. *L*:
101 Flume length. *h*: water depth. *D*₅₀: 50-th percentile of sediment GSD. *r*: experiment duration.

102

103 Apart from field data, we also benefited from the results of previous flume experiments that
104 explored the role of sediment feed reductions on the surface texture (Church et al., 1998; Hassan

506
507
508
509
510
511
512
513
514
515
516
517
518
519
520
521
522
523
524
525
526
527
528
529
530
531
532
533
534
535
536
537
538
539
540
541
542
543
544
545
546
547
548
549
550
551
552
553
554
555
556
557
558
559
560
561
562
563
564

565
566
567 and Church, 2000; Nelson et al., 2009). Table 4 describes the main characteristics of these
568
569 106 experiments. Information for these flume investigations was extracted from graphical reading of
570
571 107 figures presented in Venditti et al. (2017) (Figures 16.1, 16.2 and 16.5 in that paper).
572

573 108

575 109 **3. Review of the compiled data**

577 110 ***3.1. Surface coarsening in gravel-bed rivers: introducing the ‘armour ratio’***

578
579 111 Streambed surface is, in general, coarser than the underlying subsurface grain-size distribution
580
581 112 (GSD) in the compiled dataset: the average D_{50} and D_{84} are both coarser on the surface than the
582
583 113 subsurface GSD (Figure 1A). The degree of surface coarsening has usually been quantified in
584
585 114 fluvial geomorphology through the ‘armour ratio’ (D^*): the ratio between a characteristic grain
586
587 115 size (normally, the median size) on the surface GSD and the same characteristic grain size in the
588
589 116 subsurface GSD (Bunte and Abt, 2001):

$$591 \quad 117 \quad D_i^* = \frac{D_{is}}{D_{iss}} \quad \text{Eq. 1}$$

592
593 118 where D_i refers to the i th-percentile of the GSD. A value of D^* equal to 1 means that the surface
594
595 119 and subsurface GSD are very similar. When the surface is coarser than the subsurface GSD, then
596
597 120 $D^* > 1$; the coarser the surface is compared to the subsurface GSD, the larger the D^* . Average
598
599 121 armour ratios are larger in the compiled data if estimated using the median size rather than using
600
601 122 the D_{84} (~ 3.1 against ~ 1.8 , respectively) (Figure 2), outlining that differences between both GSD
602
603 123 are more important towards finer size fractions. In addition, some different tendencies could be
604
605 124 appreciated according to channel morphology (Figure 3).

606
607 125 Apart from surface coarsening, some other complementary trends can be identified and seem
608
609 126 intimately related to the former (Figures 1C and 1D). For instance, the percentages of fine
610
611 127 sediment are, on average, larger in the subsurface ($\sim 15\%$) than on the surface GSD ($\sim 6\%$) (Figure
612
613 128 1D). Furthermore, patterns of grain-size sorting also show differences: D_{84}/D_{50} sorting indexes
614
615 129 are again larger in the subsurface (~ 3.6 on average) than on the surface GSD (~ 2.1 on average),
616
617 130 suggesting that subsurface GSD is more poorly sorted (Figure 1C). All these differences are
618
619 131 statistically significant (Welch’s t-test for unequal variances, p-value <0.05).

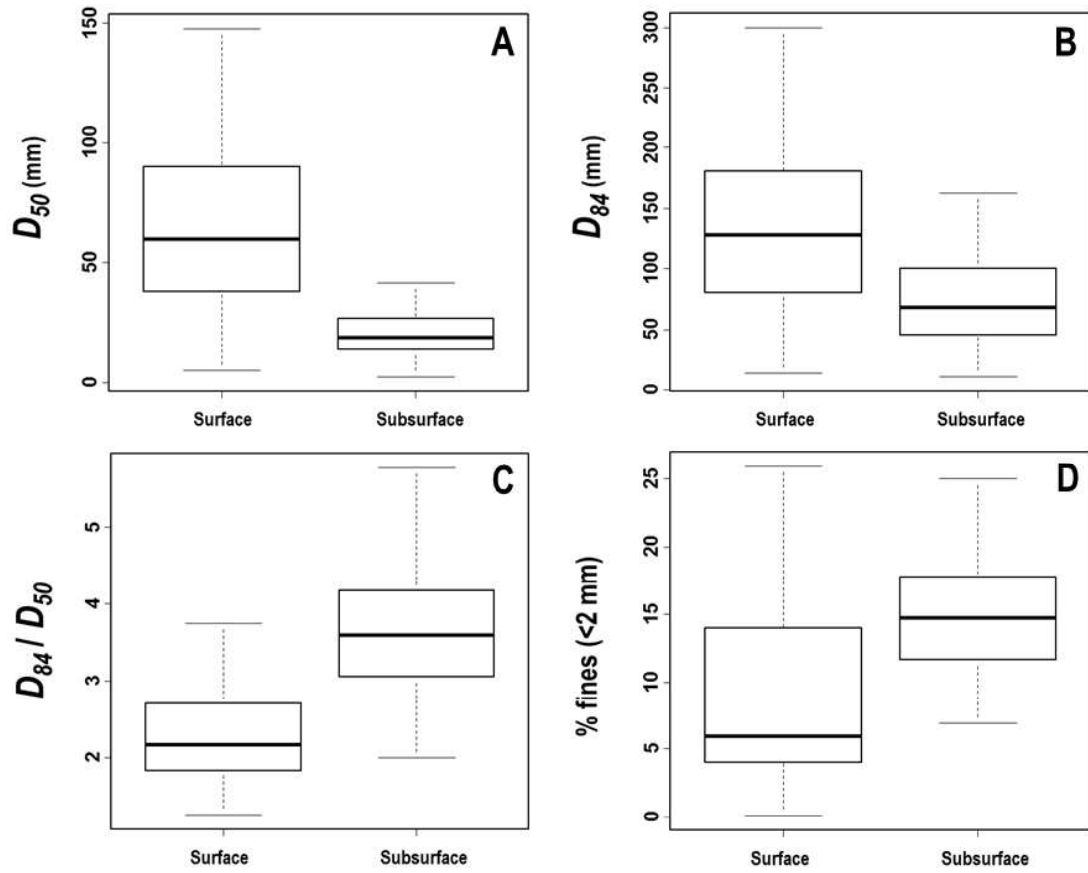


Figure 1. Comparison between surface and subsurface grain-size parameters in the compiled database. A: D_{50} (in mm); B: D_{84} (in mm). C: D_{84}/D_{50} ratio. D: Percentage of fines (< 2mm) present in the sediment.

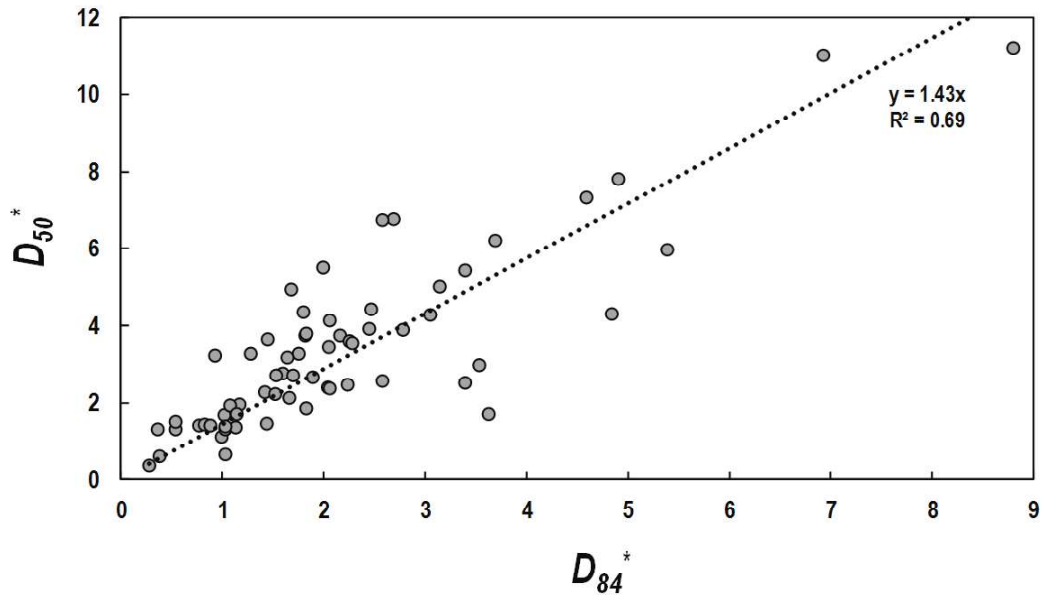


Figure 2. Armour ratios based on D_{50} plotted versus the armour ratios based on D_{84} .

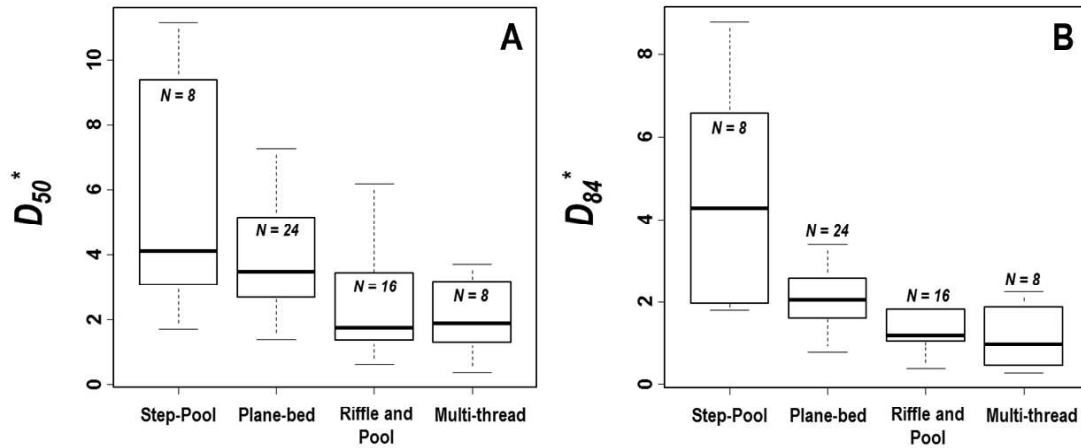


Figure 3. Differences in armour ratios according to channel morphology. A: Armour ratio based on the media size of the bed sediment (D_{50}). B: Armour ratio based on the 84-th percentile (D_{84}) of the grain-size distribution (GSD). N : Number of data.

132

133 It could initially be thought that methodological biases may explain a part of these trends.

134 Subsurface GSD is commonly determined by sieving dredged or excavated bulk volume samples

135 (Church et al., 1987). Conversely, a wide diversity of methods have been proposed to approach

136 the surface GSD, such as the classical Wolman (1954) pebble-count method, the photosieving

137 approach (Ibbeken and Schleyer, 1986, Butler et al., 2001, Rubin, 2004, Graham et al., 2005,

138 Buscombe, 2008, Detert and Weitbrecht, 2013) or the more recent protocols based on high-

139 resolution topography (e.g. Heritage and Milan, 2009; Brasington et al., 2012; Vázquez-Tarrió et

140 al., 2017; Woodget et al., 2017). Grain sizes determined from area-by-weight sample methods

141 (like the photosieving approach) are not directly equivalent to grain sizes determined from

142 volume-by-weight sampling procedures (e.g. size sieving of bulk volume samples) (Kellerhals

143 and Bray, 1971; Bunte and Abt, 2001). However, in the study cases compiled here, surface GSD

144 was generally sampled using a grid-by-number pebble count, while subsurface GSD was always

145 obtained from one variant or another (dredging, digging, frozen cores...) of the bulk volume

146 sampling strategy (Table 1). Particle-size distributions determined from volume-by-weight (size-

147 sieving of bulk volume samples) and grid-by-number (pebble count) samples are said to be

148 equivalent (Kellerhals and Bray, 1971; Bunte and Abt, 2001; Rice and Haschenburger, 2004), and

742
743
744
745
746
747
748
749
750
751
752
753
754
755
756
757
758
759
760
761
762
763
764
765
766
767
768
769
770
771
772
773
774
775
776
777
778
779
780
781
782
783
784
785
786
787
788
789
790
791
792
793
794
795
796
797
798
799
800

149 so surface coarsening seems to be a real trend in the compiled data, and not an artefact issuing
150 from methodological biases.

151 ***3.2. Sediment supply vs. hydrologic controls on surface coarsening and ‘armour ratios’***

152 The grain size of sediment inputs should exert an obvious control on the grain calibre of the
153 available bed material within a specific river reach, which in turn may condition the sediment size
154 of the streambed’s surface. In this regard, we could consider subsurface GSD as a proxy for the
155 GSD of the average annual sediment inputs (Kuhnle and Willis, 1992; Lisle, 1995; Church and
156 Hassan, 2005; Recking, 2013; Segura and Pitlick, 2015), i.e. the GSD available in the subsurface
157 should condition the GSD of the streambed surface. Within the compiled data, we observe some
158 statistically significant and moderate correlation between surface and subsurface GSD (Figure 4),
159 which highlights this undeniable influence of the sediment supply GSD on the GSD of the
160 streambed’s surface. However, it is interesting to notice how variance in grain-size data is larger
161 for surface than subsurface GSD (see Figures 1A and B). This suggests that grain-size variability
162 introduced by the sediment supplies is diluted by the variability in surface coarsening introduced
163 by some other controls.

164 In this regard, the compiled data show some statistically significant differences (ANOVA test, p-
165 value < 0.05) in armour ratios according to the amounts of sediment supply at the catchment scale
166 (Figure 5): rivers with high sediment supplies tend to show lower armour ratios than streams with
167 low sediment feeds. Surface coarsening (often named ‘armouring’) has been described in gravel-
168 bed settings for a long time (e.g. Gessler, 1967), and already related to the higher or lower
169 availability of upstream sediment inputs. Armouring has been, thereby, typically reported in
170 degrading beds and river reaches with low or no sediment supply (e.g. gravel-bed reaches below
171 dams or lakes) (Gessler, 1967; Willets et al., 1988; Chin et al., 1994; Gomez, 1994; Vericat et al.,
172 2006). In such cases, armouring is called ‘static’ or ‘pavement’ (Jain, 1990; Yager et al., 2015;
173 Bertin and Freidrich, 2018). Static armours can ‘break up’ during high peaks of flow and/or
174 transport episodes with large sand sediment supplies (Laronne and Carson, 1976; Gomez, 1983;
175 Klaasen, 1988; Chin et al., 1994; Venditti et al., 2005; Vericat et al., 2006; Wang and Liu, 2009;
176 Venditti et al., 2010; Spiller et al., 2012; Curran and Waters, 2014; Orrú et al., 2016; Bertin and

177 Freidrich, 2018) and re-form during the falling limb of the flood hydrograph, together with a
 178 progressive reduction in sediment mobility and the winnowing of finer and more mobile particles
 179 (Mao, 2012).

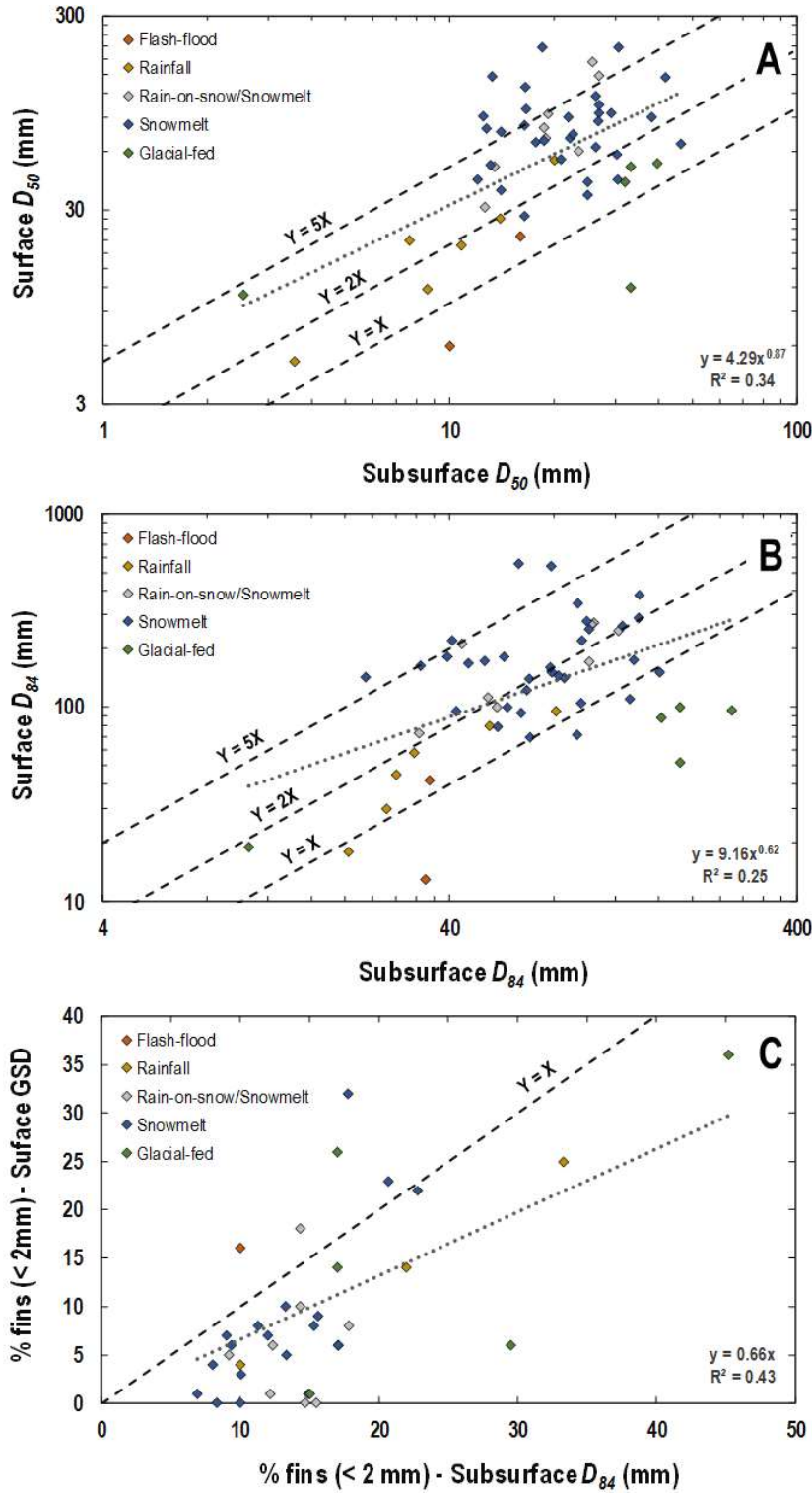


Figure 4. Surface grain-size parameters plotted versus subsurface parameters. A: D_{50} . B: D_{84} . C: Percentage of fine sediment (< 2 mm). We have segregated the data according to hydrological regime.

180

181

853

854

855

856

857

858

859

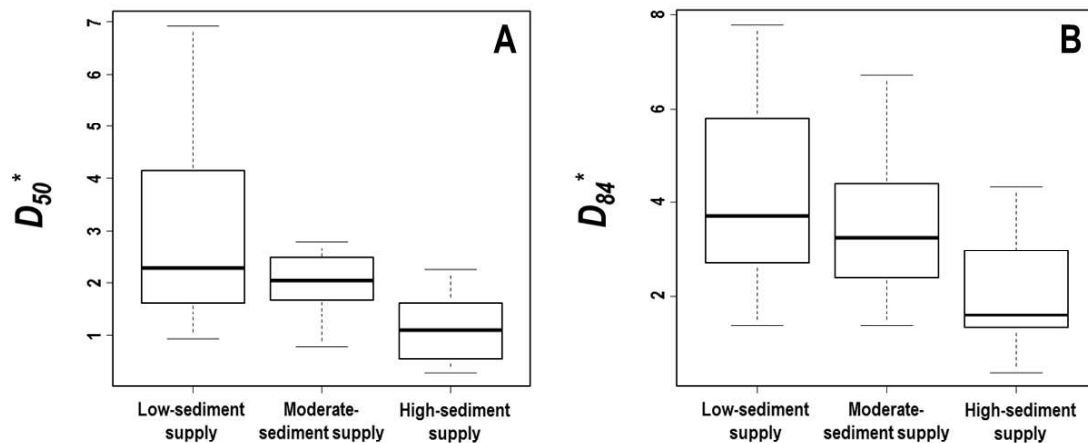


Figure 5. Differences in armour ratios according to sediment-supply conditions at the catchment scale. See main text. A: D_{50}^* . B: D_{84}^* .

182

183 However, the compiled data illustrate how a certain degree of surface armouring ('armour ratios'
 184 >1) can also be observed in rivers fed by significant sediment supplies (Figure 5). Therefore, non-
 185 degrading gravel-bed streams with considerable sediment inputs may also exhibit some
 186 armouring. In truth, bedload transport models (Wilcock and DeTemple, 2005), tracer studies
 187 (Haschenburger and Wilcock, 2003), flume experiments (Hassan et al., 2006), and field
 188 observations (Andrews and Erdman, 1986; Clayton and Pitlick, 2008; Haschenburger, 2017)
 189 support the occurrence of such 'mobile' armours and suggest their persistence even during large
 190 floods. The sheltering of small particles into pockets and interstices between coarse grains can
 191 contribute to the development of these coarsened surfaces in well-supplied rivers (Parker et al.,
 192 1982; Parker and Klingeman, 1982; Andrews and Erman, 1986; Andrews and Parker, 1987; Berni
 193 et al., 2018). Surface coarsening represents in these cases an effective mechanism allowing for
 194 the transport of the coarse fractions in the gravel load at the same rate as those which are finer
 195 (Parker and Klingemann, 1982; Parker and Toro-Escobar, 2002; Parker, 2004). As such, it leads
 196 to a progressive equalization between the bedload and the subarmour GSDs (Parker and
 197 Klingemann, 1982; Marion and Fraccarollo, 1997; Mario et al., 2003; Mao et al., 2011; Powell et
 198 al., 2016; Bertin and Freidrich, 2018), a situation referred to as 'dynamic' or 'mobile armours'.
 199 Moreover, in gravel-bed rivers, the amount of entrained bed material and the grain size of the
 200 bedload increase as flow discharge rises (Milhous, 1973; Jones and Seitz, 1980; Kuhnle and

919
920
921
922
923
924
925
926
927
928
929
930
931
932
933
934
935
936
937
938
939
940
941
942
943
944
945
946
947
948
949
950
951
952
953
954
955
956
957
958
959
960
961
962
963
964
965
966
967
968
969
970
971
972
973
974
975
976
977

201 Willis, 1992; Andrews, 1994; Wathen et al., 1995; Powell et al., 2001; Ryan and Emmett, 2002;
202 Wilcock and McArdell, 1993, 1997; Clayton and Pitlick, 2008; Pitlick et al., 2008; Recking,
203 2016). We could, thereby, expect differences in mobility between different grain-size classes with
204 fluctuations in flow discharge. Therefore, selective transport and horizontal winnowing of fines
205 during recession limbs and/or low flows may exhaust the fine sediment and favour the
206 development of a cover of coarse material preventing further sediment transport (Harrison, 1950;
207 Gessler, 1970; Little and Mayer, 1972; Proffitt and Sutherland, 1983; Chin et al., 1994). In this
208 regard, perennial and seasonal streams subjected to long-lasting floods and sustained receding
209 limbs might have more chances of suffering a coarsening of their bed surfaces and thus become
210 more armoured. In the opposite extreme, we could consider streams experiencing flashing-flood
211 hydrology. A flash flood involves a sudden increase of peak flows, bed shear stresses and equal
212 mobility for all the particle sizes represented in the streambed (Laronne and Reid, 1993; Laronne
213 et al. 1994; Reid and Laronne, 1995). In such cases, we should not expect large differences
214 between the surface, subsurface and bedload GSDs (Dietrich et al., 1989; Chin et al., 1994; Powell
215 et al., 2001; Parker, 2008; Venditti et al., 2017; Bertin and Friedrich, 2018). As a result, streams
216 receiving comparable amounts of sediment inputs may exhibit different armour ratios depending
217 on the dominant hydrological regime (Hassan et al., 2006).

218 Unfortunately, the compiled data are mostly from mountain streams dominated by snowmelt flow
219 regimes, probably because planning field-campaigns in order to measure bedload is easier in this
220 kind of rivers compared to rainfall-dominated settings, where it is more difficult to know in
221 advance when a channel-forming flow is going to occur (also to monitor within a fairly deep flow
222 channel with long rising and falling limbs). Thus, it is not easy to explore in depth the influence
223 of hydrological regime with the available data. In any case, snowmelt-dominated rivers, usually
224 submitted to sustained floods during the melting season, tend to show larger armour ratios than
225 rainfall or flash-flood dominated streams (see dotplot shown in Figure 6). Furthermore, the
226 percentage of fine sediment also tends to be lower in these snowmelt-dominated streams (Figure
227 6B), indicating fine sediment depletion during the long and gradually declining limbs of typical
228 snowmelt hydrographs. On the other hand, glacial-fed rivers, which normally have high-sediment

978
979
980
981
982
983
984
985
986
987
988
989
990
991
992
993
994
995
996
997
998
999
1000
1001
1002
1003
1004
1005
1006
1007
1008
1009
1010
1011
1012
1013
1014
1015
1016
1017
1018
1019
1020
1021
1022
1023
1024
1025
1026
1027
1028
1029
1030
1031
1032
1033
1034
1035
1036

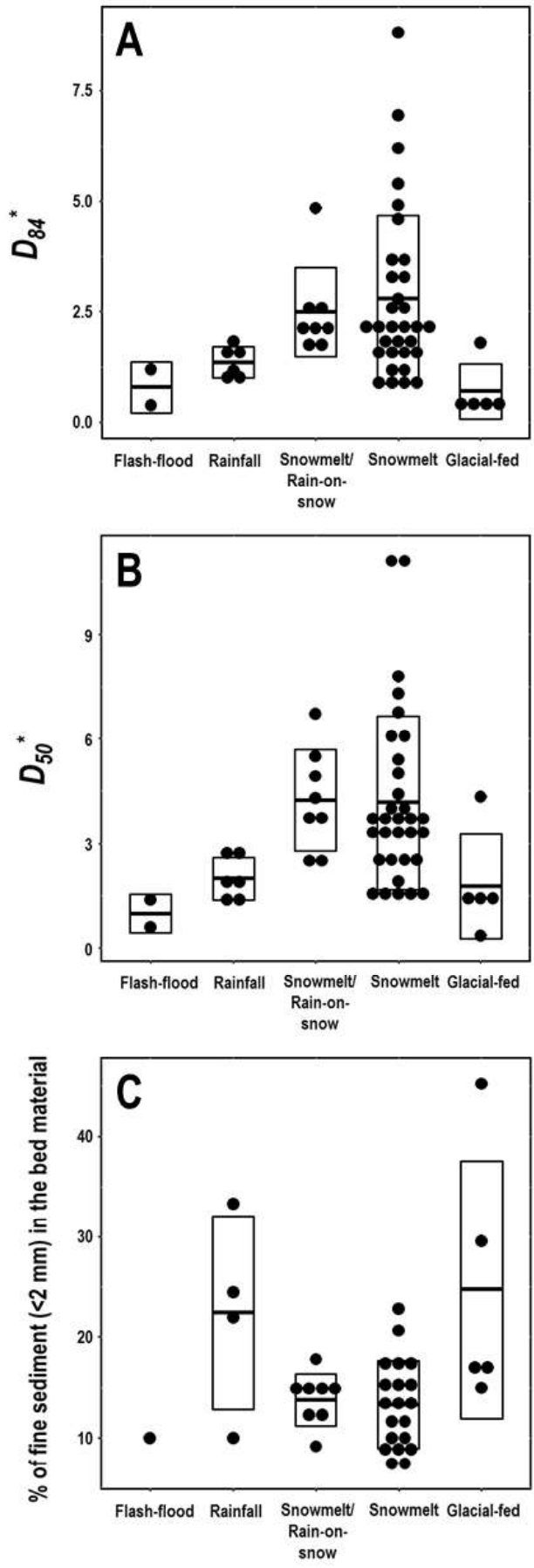


Figure 6. Differences in armour ratios (A and B) and percentages of fine sediment (C) according to the dominant flow regime.

1037
1038
1039 229 supplies from glacial/periglacial sources (particularly the 'glacial flour' transported from
1040
1041 230 glaciated upland basins), show relatively low armour ratios (Figure 6B). The influx of fine
1042
1043 231 sediments represented by the glacial flour may help the coarse grains composing the armour layer
1044
1045 232 to become more mobile (Cui et al., 2003; Venditti et al. 2010a, b; Yager et al., 2015). In addition,
1046
1047 233 the flow regime of glacial-fed rivers is often characterised by daily peaks of discharge, rising and
1048
1049 234 falling successively, and these somewhat shorter, rapidly changing hydrographs are less prone to
1050
1051 235 promote armouring (Hassan et al., 2006). Hence, in conjunction, both issues may determine the
1052
1053 236 relatively low armour ratios documented here in the case of glacial-fed rivers.

1054
1055 237 To summarize, our review of field data shows how sediment supply, together with the shape of
1056
1057 238 the dominant flood hydrographs, condition surface armouring in gravel-bed rivers. The
1058
1059 239 hydrological regime controls the rate at which bedload and fine sediment are winnowed and
1060
1061 240 exhausted during the course of transport events. For instance, we can expect a less armoured
1062
1063 241 surface if a continuous replenishment of sediment exists during the transport episode, as we can
1064
1065 242 reasonably expect for glacial fed streams. In the opposite extreme, we can anticipate a better
1066
1067 243 developed armouring and a streambed surface more depleted in fines in cases where the bedload
1068
1069 244 is exhausted, which is likely when streams are subjected to long-lasting snowmelt hydrographs.
1070
1071 245 This is in accordance with the set of flume experiments by Hassan et al. (2006) who investigated
1072
1073 246 the influence of different hydrographs on surface armouring and observed varying textural
1074
1075 247 responses to steady vs. gradually varying flows. Nevertheless, fine sediment depletion during
1076
1077 248 floods may take more or less time depending on the amount of sediment supplied from upstream
1078
1079 249 sources. Therefore, the rate at which bedload is supplied into the channel may modulate the effects
1080
1081 250 of flow hydrographs and strongly determine the rate and degree of fine sediment depletion, and
1082
1083 251 consequently the degree of armour development.

1084 252 ***3.3. Surface armouring and streambed mobility***

1086 253 As stated above, surface coarsening is associated with fine sediment exhaustion from the
1087
1088 254 streambed and the development of clast arrangements and imbrications (Church et al., 1998;
1089
1090 255 Venditti et al., 2017). The increase of particle stability linked to surface structuration may involve
1091
1092 256 a decrease in the frequency of clast mobility and streambed disorganization (Church et al., 1998;
1093
1094
1095

1096
 1097
 1098 Hassan and Church, 2002). To further explore this issue, we introduce a new metric: the ‘transport
 1099
 1100 stage’ ratio (τ^*/τ_c^*). This is defined as the ratio between the peak basal shear stress for a given
 1101
 1102 259 flow discharge and its critical value for incipient sediment motion. Critical stresses for sediment
 1103
 1104 260 entrainment were estimated here based on Recking’s (2013) fit for D_{84} (see supplementary files
 1105
 1106 261 for more information about how we computed transport stage ratios).

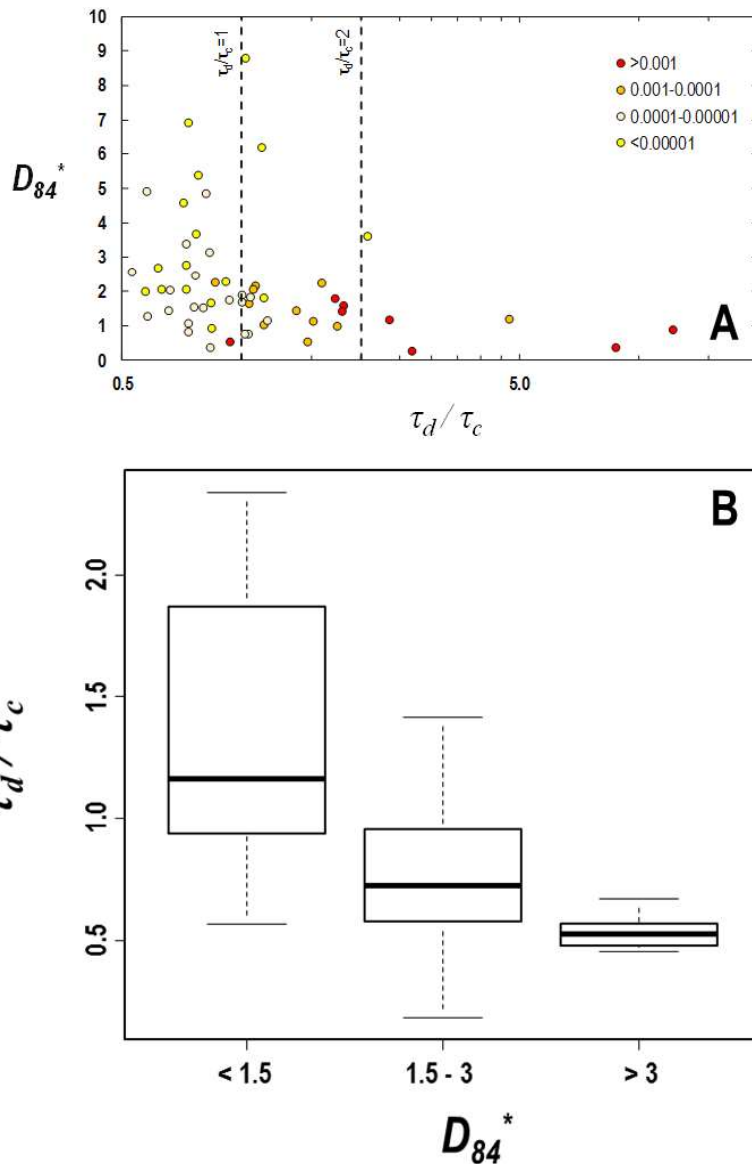


Figure 7. A: Armour ratio (D_{84}^*) plotted versus the transport stage (τ_d/τ_c). B: Transport stages values at the dominant discharge in poorly armoured ($D_{84}^* < 1.5$), normally armoured ($1.5 < D_{84}^* < 3$) and well armoured ($D_{84}^* > 3$) rivers. Critical threshold Shields values (τ_c) were computed using Recking, 2009).

1143 262 Values of this metric, estimated at the dominant channel-forming discharge, are close to the
 1144
 1145 263 critical thresholds for entrainment of the coarser fraction of bed sediment in well-armoured
 1146
 1147 264 streams (Figure 7A). However, in poorly armoured streams, Shields stresses are well above these
 1148
 1149 265 critical values. These poorly armoured streams also show larger bedload fluxes (see the values
 1150
 1151 266 for transport intensities in Fig. 7A). A turning point can be defined close to an armour ratio of ~2:

1096
 1097
 1098
 1099
 1100
 1101
 1102
 1103
 1104
 1105
 1106
 1107
 1108
 1109
 1110
 1111
 1112
 1113
 1114
 1115
 1116
 1117
 1118
 1119
 1120
 1121
 1122
 1123
 1124
 1125
 1126
 1127
 1128
 1129
 1130
 1131
 1132
 1133
 1134
 1135
 1136
 1137
 1138
 1139
 1140
 1141
 1142
 1143
 1144
 1145
 1146
 1147
 1148
 1149
 1150
 1151
 1152
 1153
 1154

1155
1156
1157 267 there are no channels with large transport intensities ($\phi > 0.0001$) and high transport stages at
1158
1159 268 dominant discharge ($\tau^*/\tau_c^* > 2$) for armour ratios larger than 2. These observations confirm that
1160
1161 269 overall streambed mobility would be larger in poorly armoured streams, and document how well-
1162
1163 270 armoured streambed surfaces are seldom moved. Considering all of the above, the compiled data
1164
1165 271 support the idea of surface armouring being conditioned by dominant sediment supply conditions
1166
1167 272 (section 2.2), with ‘static-armours’ characterised by larger armour ratios than ‘mobile-armours’
1168
1169 273 (Figure 7B).

1171 274 **3.4. Quantifying sediment supply conditions in gravel-bed rivers**

1172
1173 275 Our review of the literature clearly shows how the GSD of a streambed’s surface, at a given river
1174
1175 276 reach, adjusts to the volume of sediment inputs and the ability of the channel to export the
1176
1177 277 available sediment inputs (Figures 6 and 7), an idea already outlined by previous field and flume
1178
1179 278 studies (Dietrich et al., 1989; Venditti et al., 2017). Introducing metrics allowing the quantitative
1180
1181 279 description of the sediment supply is then of interest as shown by Dietrich et al. (1989) who
1182
1183 280 proposed their own metric (q^*) (Dietrich et al., 1989; Montgomery and Buffington, 1997; Venditti
1184
1185 281 et al., 2017):

$$1186 \quad 282 \quad q^* = \frac{q_{s_s}}{q_{s_{ss}}} \quad \text{Eq. 2}$$

1187
1188
1189 283 where q_s refers to the bedload transport rate per unit width and the subscripts s and ss to the surface
1190
1191 284 and subsurface sediment, respectively. The ‘bedload supply’ index as defined in eq. 2 is the ratio
1192
1193 285 between the sediment transport capacity to mobilize the surface GSD and the capacity to recruit
1194
1195 286 sediment from a hypothetical surface as fine as the subsurface. When actual bedload rates match
1196
1197 287 the bedload transport capacity of the channel, q^* should equal 1. Conversely, if sediment inputs
1198
1199 288 into the channel are lower than transport capacities, then $q^* < 1$. Here we computed the q^* ratio,
1200
1201 289 based on flow characteristics at the representative channel-forming discharge and on Recking’s
1202
1203 290 equation (details on q^* calculation are explained in the supplementary information, Subsection
1204
1205 291 S.3). The obtained values of q^* are in good agreement with our initial classification of compiled
1206
1207 292 data as high-, moderate- and low-sediment supplied channels (Figure 8A).

1214
 1215
 1216 293 However, the ‘bedload supply’ index q^* has the problem of estimating bedload transport capacity
 1217
 1218 294 of a channel for a hypothetical situation where the streambed’s surface GSD equals its subsurface
 1219
 1220 295 GSD (q_{ss} , denominator in eq. 2). In the field cases compiled here, this required the application of
 1221
 1222 296 a bedload equation for the estimation of q_{ss} , with all the uncertainties linked to choosing the right
 1223
 1224 297 formula. For that reason, we propose a simpler metric to quantify the ratio between the flux of
 1225
 1226 298 sediment entering a given river reach, and the capacity of the channel to transport that sediment
 1227
 1228 299 downstream: the ratio between bedload fluxes (q_s) and stream power (ω) at the representative or
 1229
 1230 300 dominant channel-forming discharge. This metric quantifies the mass of sediment carried by a
 1231
 1232 301 river with a given amount of hydraulic power. Values of this ratio are in good agreement with our
 1233
 1234 302 initial classification of the compiled data as high-, moderate- and low-sediment supply channels
 1235
 1236 303 (Figure 8B), confirming its usefulness for characterizing the dominant sediment supply conditions
 1237
 1238 304 in gravel-bed rivers.

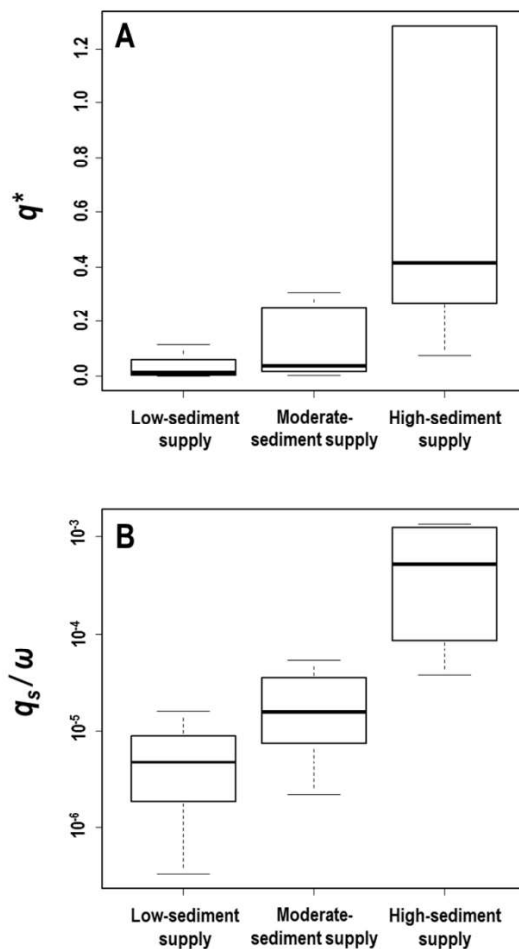


Figure 8. Differences in sediment-supply metrics (q^* and q_s/ω) according to our initial classification of data as low-, moderate- or high-sediment supply streams (see the main text). A: sediment supply metrics proposed by Dietrich et al. (1989). B: our own sediment supply metrics (see main text).

1273
1274
1275 305 **4. Meta-analysis on the data: linking streambed texture, sediment supply and hydrological**
1276
1277 306 **regime**

1279 307 **4.1. Surface armouring driven by sediment supply**

1281 308 Based on their own flume experiments, Dietrich et al. (1989) already observed that D^* increases
1282
1283 309 while sediment feed decreases compared to the overall bedload transport capacity of the channel.
1284
1285 310 Using Meyer-Peter and Muller's (1948) bedload transport equation, these authors described the
1286
1287 311 links between surface armouring (D_{50s}/D_{50ss}) and sediment supply (q^*) as:

1289
1290 312
$$q^* = \left(\frac{\frac{\tau}{\tau_{css}} - D_{50}^*}{\frac{\tau}{\tau_{css}} - 1} \right)^{1.5} \quad \text{Eq. 3}$$

1291

1293 313 where τ is the basal shear stress and τ_{css} is the critical shear stress for the inception of motion in
1294
1295 314 the subsurface sediment. At the time when Dietrich et al. (1989) published their work, using
1296
1297 315 Meyer-Peter and Muller's (1948) bedload equation made sense due to its simplicity and its
1298
1299 316 common use in sediment transport studies. However, more sophisticated bedload transport
1300
1301 317 formulas have been proposed since then (e.g. Wilcock and Crowe, 2003; Recking, 2013), which
1302
1303 318 proved to perform well for 1D computations of bedload in natural gravel-bed streams (e.g. Parker,
1304
1305 319 2004; Recking, 2010; Camenen et al., 2011; Vázquez-Tarrío and Menéndez-Duarte, 2015; Hinton
1306
1307 320 et al., 2018). In this paper, based on Recking's (2013) (after Recking et al., 2016) bedload
1308
1309 321 equation, the following expressions are obtained (see details in the supplementary information):

1310
1311 322
$$D_{84}^* = \frac{1}{f} \cdot q^{*-1/5} \quad \text{for partial-mobility conditions} \quad \text{Eq. 4}$$

1312

1313
1314 323
$$D_{84}^* = q^{*-1} \quad \text{for full-mobility conditions} \quad \text{Eq. 5}$$

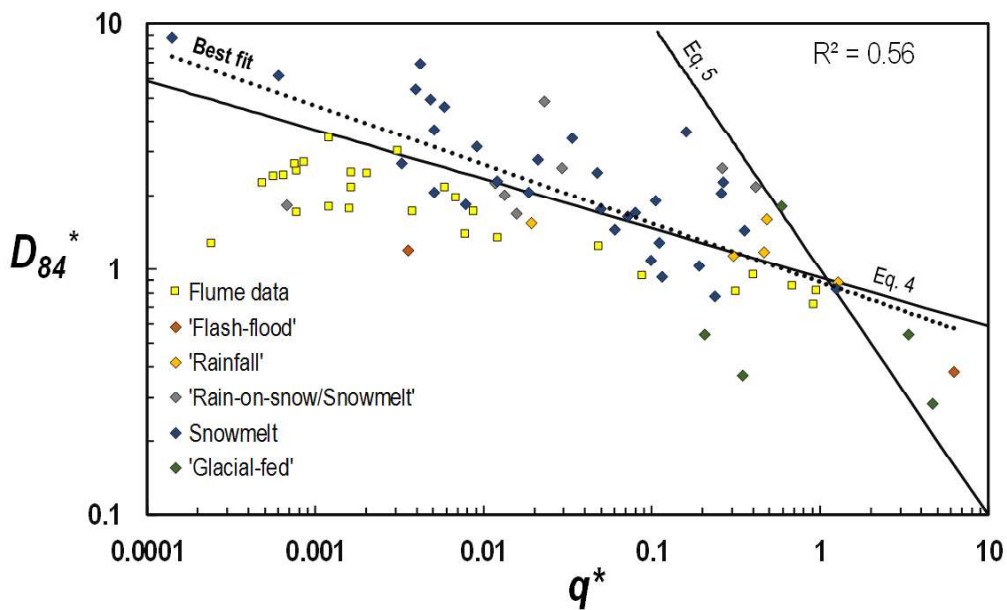
1315
1316 324 where f in eq. 4 is a parameter relating D_{50}^* to D_{84}^* (~ 1.4 , according to Figure 2). Eqs. 4 and 5
1317
1318 325 provide a simple mathematical description of how D^* should correlate and change with q^* . As
1319
1320 326 opposed to eq. 3, eqs. 4 and 5 use D_{84}^* rather than D_{50}^* , because Recking's (2013) equation works
1321
1322 327 with the 84-th percentile of the surface GSD as the reference bed sediment size.

1323
1324 328 In Figure 9 we have plotted D_{84}^* against q^* for the field data, the latter estimated from flow
1325
1326 329 characteristics at the dominant channel-forming discharge and Recking's equation (details on q^*
1327
1328 330 calculation are explained in the supplementary information). We have also incorporated into this

1332 plot data from flume experiments (extracted from Venditti et al., 2017; see supplementary
 1333 information), which tend to overlap the field data: armour ratios change with bedload supply
 1334 following a similar trend in flume and field data. Additionally, the obtained fit is very close to the
 1335 curve defined by eq. 4 (low-transport stage conditions). This suggests that partial mobility
 1336 conditions may dominate bedload motion at the dominant discharge in well-armoured streams.
 1337 We also plotted armour ratios against q_s/ω ratios (Figure 10A), and the data show a moderate but
 1338 statistically significant correlation between the q_s/ω ratio and the armour ratios. As shown above
 1339 (Figure 4), D_s is partially controlled by D_{ss} . This covariation may be introducing some noise in
 1340 the plot shown in Figure 10A. In order to remove this effect, we propose a new version of the
 1341 armour ratio (D^{**}):

$$D^{**} = \frac{D_s}{D_{ss}^\beta} \quad \text{Eq. 6}$$

1342 where β is the parameter defining how surface grain-size scales to subsurface grain-size.
 1343 According to Figure 4, β is ~ 0.62 and ~ 0.41 for D_{84} and D_{50} , respectively. This ‘corrected’ version
 1344 of the armour ratio shows a stronger correlation to the q_s/ω ratio (Figure 10B). Similar to Figure
 1345 9, Figure 10 shows how streambed surface tends to coarsen with decreasing sediment supplies
 1346 (proxied here by the q_s/ω ratios).



1385 **Figure 9.** Armour ratio plotted against the ‘bedload supply ratio’ q^* (see main text for more
 1386 details).
 1387
 1388
 1389
 1390

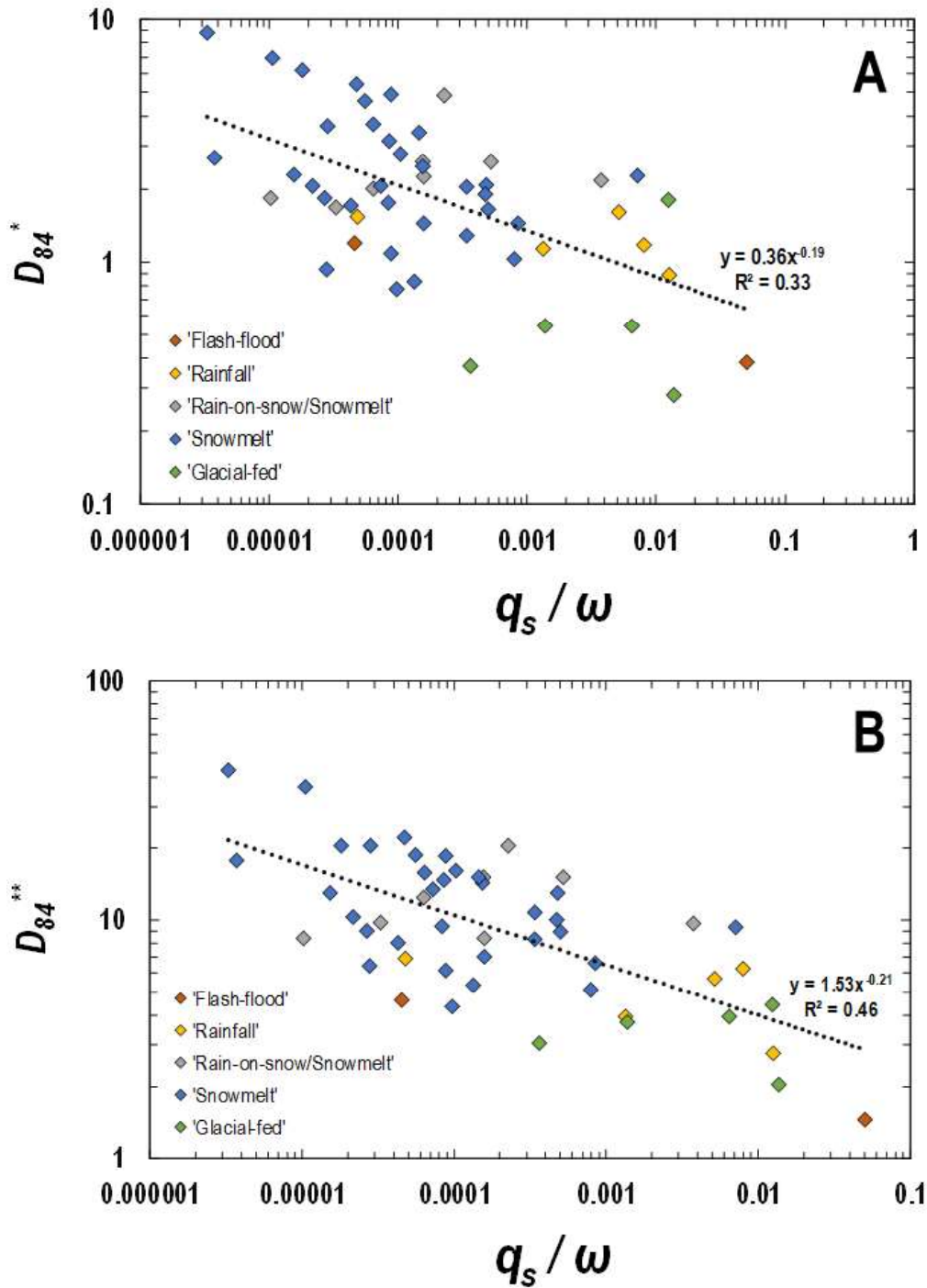


Figure 10. Armour ratio (A) and corrected armour ratio (B) plotted versus the ratio between bedload fluxes and streampower (q_s/ω_d).

347

348 Although the number of plots is not well balanced across the different groups of data, it is worth
 349 pointing out that in Figures 9 and 10 rainfall data tend to plot close to the regression line, while
 350 snowmelt data tend to show a larger scatter and broader range of armour ratios. Snowmelt systems
 351 are typically located in the upper parts of the catchment compared to rainfall streams, which are

1447

1448

1449

1450
1451
1452 352 usually located downstream, further from the coarser sediment sources. Consequently, this
1453
1454 353 implies that rainfall streams will be somewhat less prone to develop larger armour ratios even if
1455
1456 354 their sediment supply is limited. In this regard, large armour ratios may have some dependence
1457
1458 355 on the upstream/downstream location of the stream and its particular geological context, as
1459
1460 356 already suggested by Pitlick et al. (2008).

1462 357 ***4.2. Hydrological controls on surface armouring***

1463
1464 358 Figures 9 and 10 clearly show how streambed surface evolves and becomes progressively
1465
1466 359 armoured with declining sediment supplies. Nevertheless, there is a certain amount of scatter in
1467
1468 360 both plots, which highlights that some variability in armour ratios may exist with a given sediment
1469
1470 361 supply. Indeed, data from snowmelt streams tend to plot in the upper envelope of the point cloud
1471
1472 362 in Figure 9 and, conversely, data from glacial-fed and flash-flood dominated streams tend to fall
1473
1474 363 in the lower envelope, while flume data project in the middle of the point cloud, together with
1475
1476 364 rainfall dominated rivers. Similarly, in Figure 6 snowmelt dominated streams tend to show larger
1477
1478 365 armour ratios and smaller q_s/ω ratios than rainfall, flash flood and glacial-fed dominated streams.
1479
1480 366 All these observations highlight the variability in surface armouring and sediment supply
1481
1482 367 conditions and their interplay with different hydrological regimes.
1483
1484 368 However, we should also consider that adjustments of the streambed to shifts in sediment supply
1485
1486 369 conditions are not always synchronous and there is potentially a lag between the two. For instance,
1487
1488 370 surface coarsening slowly propagates downstream after widespread land cover changes in the
1489
1490 371 upland basin or downstream from a dam (Rollet et al., 2013), so it can take several years before
1491
1492 372 we observe riverbed coarsening following a significant upstream perturbation. Furthermore, in
1493
1494 373 snowmelt systems, some hysteresis in bedload supplies can be observed over the hydrological
1495
1496 374 year (Moog and Whiting, 1998); for instance, there can be significant bedload transport for a
1497
1498 375 given discharge in early spring, while bedload rates are reduced for similar flow discharges
1499
1500 376 occurring at the end of the flood season (Misset et al., in press). We have not controlled for all
1501
1502 377 these variables, so they probably introduce additional scatter in the relations between surface
1503
1504 378 armouring and sediment supply reported here.

1509
1510
1511 379 **4.3. Quantifying the variability in armour ratios**
1512

1513 380 Based on the analysis performed in Subsections 4.1 and 4.2, we can conclude that surface
1514
1515 381 coarsening accommodates to the dominant sediment supply conditions, but the rate at which
1516
1517 382 bedload is emptied during the course of transport episodes may modulate the streambed
1518
1519 383 adjustment to sediment supply. This may complicate the use of armour ratio for river diagnosis,
1520
1521 384 insofar as the dominant sediment supply conditions are not the only drivers of surface grain-size
1522
1523 385 in gravel-bed rivers. The rate at which fine bedload exhausts during floods, the seasonal
1524
1525 386 variability in sediment availability and the time lag before the riverbed starts to respond after a
1526
1527 387 significant shift in the upstream bed material supplies also have a non-negligible impact on the
1528
1529 388 armour ratios documented at a given river reach. All these constraints may be largely dependent
1530
1531 389 on site-specific controls, such as the cross-sectional extent of armour break-up, the shape and
1532
1533 390 duration of the flow hydrograph, and the local availability of loose and fine sediment coming
1534
1535 391 from upstream reaches and bank toes.

1536 392 In this regard, Figures 9 and 10 not only illustrate how surface coarsening scales with sediment
1537
1538 393 supply, but also show the range of potential variability in armour ratios for a given sediment
1539
1540 394 supply and observed within the compiled field data. That said, we could report rivers more or less
1541
1542 395 armoured than the streambed conditions expected for an ‘average behaviour’ with a given bedload
1543
1544 396 input, reminiscent of the old distinction between ‘static’ versus ‘mobile’ armours (Jain, 1990;
1545
1546 397 Parker and Sutherland, 1990), so we refer to more (or less) mobile armour layers than the average
1547
1548 398 mobility expected for a given sediment supply condition (defined by the best fit in Figures 9 and
1549
1550 399 10). To handle this variability, we performed a quantile regression analysis and plotted the
1551
1552 400 regression between the different percentiles of the D^* distribution and the sediment supply metrics
1553
1554 401 (q^* and q_s/ω), obtaining two diagrams that illustrate the likelihood of a given value of D^* (Figure
1555
1556 402 11A) or D^{**} (Figure 11B) with a given sediment supply. Fluctuations from the 1-st to the 99-th
1557
1558 403 percentiles are linked to a set of factors, which include differences in the hydrological regime,
1559
1560 404 seasonal variability and time passed after significant shifts in upstream sediment inputs. Thus,
1561
1562 405 Figures 11A and 11B can be easily combined with some available qualitative information on a
1563
1564
1565
1566
1567

1568
1569
1570 406 specific study site in order to have an idea of the most probable values for the armour ratio with
1571
1572 407 a given sediment supply and hydrological regime.
1573
1574
1575
1576
1577
1578
1579
1580
1581
1582
1583
1584
1585
1586
1587
1588
1589
1590
1591
1592
1593
1594
1595
1596
1597
1598
1599
1600
1601
1602
1603
1604
1605
1606
1607
1608
1609
1610
1611
1612
1613
1614
1615
1616
1617
1618
1619
1620
1621
1622
1623
1624
1625
1626

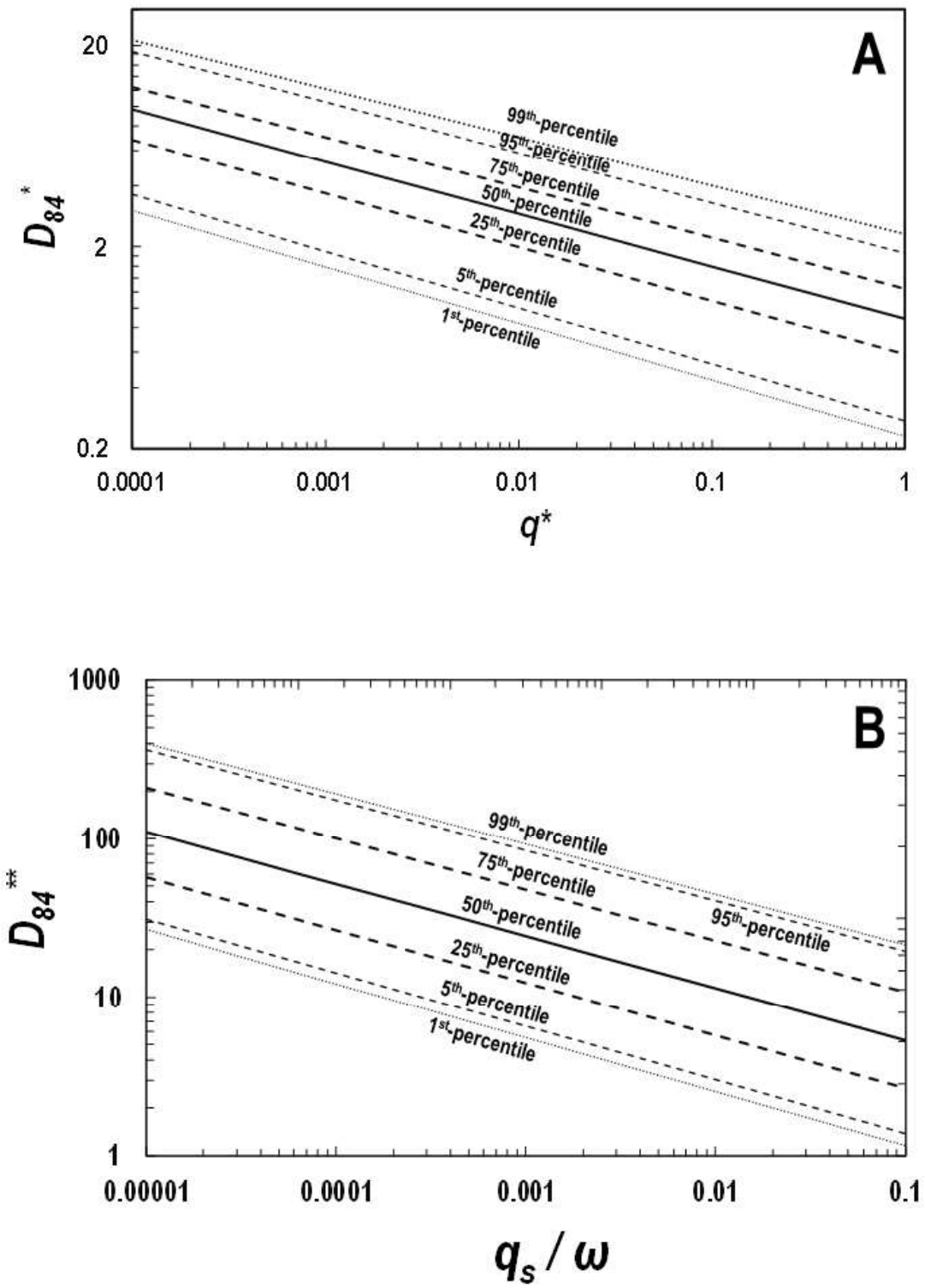


Figure 11. Diagrams issued from quantile regression analysis of the compile data, defining the likelihood of a certain value of the armour ratio according to sediment supply metrics (see main text for more details).

1627
1628
1629 408 **4.4. Studying links between bedload transport, channel morphology and surface armouring**
1630

1631 409 Streambed surfaces adjust to available bedload yields (Figures 9 and 10). Reciprocally, surface
1632
1633 410 coarsening controls the frequency and magnitude of armour breakup and streambed
1634
1635 411 disorganization during floods (Figure 7). Strongly armoured streambeds are more difficult to
1636
1637 412 disorganize and more infrequently moved. Therefore, we could expect a lower degree of bed
1638
1639 413 material recruitment into bedload during regular flows. With this in mind, we expected surface
1640
1641 414 armouring to have some control over bedload rates. In order to explore this issue, we took the
1642
1643 415 available information on bedload discharges (Table 1) and performed a multiple regression
1644
1645 416 analysis linking bedload rates to flow magnitude and armour ratios:

1646
1647 417
$$\phi = \left(Q/Q_d\right)^a \cdot (D_{84}^*)^b \quad \text{Eq. 7}$$

1648

1649 418 where ϕ is bedload transport intensity (see supplementary information), and Q/Q_d is the ratio
1650
1651 419 between the peak discharge for the transport episode and the dominant discharge (hereinafter
1652
1653 420 called flow ratio). However, the wide diversity of channel morphologies represented amongst the
1654
1655 421 compiled data should be highlighted, since channel macroforms control flow and sediment
1656
1657 422 transport patterns, which in turn may potentially affect bedload rates (Ferguson, 2003; Francalanci
1658
1659 423 et al., 2012; Recking et al., 2016; Vázquez-Tarrío et al., 2018; Vázquez-Tarrío and Batalla, 2019).
1660
1661 424 For this reason, we introduced a set of three binary indicators into the regression analysis to
1662
1663 425 incorporate into it the influence of channel morphology:

1664
1665 426
$$\phi = \left(Q/Q_d\right)^a \cdot (D_{84}^*)^b \cdot e^{c \cdot RP} \cdot e^{d \cdot SP} \cdot e^{d \cdot BR} \quad \text{Eq. 8}$$

1666
1667

1668 427 where RP, SP and BR are the dummy variables taking a value of 1 in the cases of riffle and pool,
1669
1670 428 step-pool and braided channels, respectively. In the case of plane-bed channels, the three dummy
1671
1672 429 variables would be 0.

1673
1674 430 To test whether eqs. 7 and 8 fit the available bedload information, we used ordinary multiple
1675
1676 431 regression in linearized form and stepwise procedures, after log transforming all the variables
1677
1678 432 included in the equation. Both equations explain the variance in the compiled bedload data to a
1679
1680 433 statistically significant degree, with all the variables included in the regression model being
1681
1682 434 significant (Table 5). The R^2 values imply that eq. 8 is more robust than eq. 7 ($R^2 = 0.60$ vs. 0.34,
1683
1684
1685

435 respectively), which outlines the existence of some morphological imprint on bedload transport
 436 rates. According to the regression model, transport intensities increase with the 1.7 positive power
 437 of flow ratios. Conversely, bedload rates are negatively correlated to armour ratios, i.e. bedload
 438 rates tend to be considerably weaker in well-armoured channels. With the aim of assessing the
 439 relative importance of each of the independent variables incorporated into the regression model,
 440 we used the method proposed by Lindeman et al. (1980), often recommended for assigning shares
 441 of relative weight of predictors to the R^2 . According to this analysis, channel morphology is the
 442 variable that explains the largest amount of variability in bedload data ($\sim 53\%$ of R^2), followed
 443 by flow magnitude (23% of R^2) and armour ratios (21% of R^2). Differences in dominant channel
 444 morphology have a strong effect on the variability in bedload rates observed between the
 445 compiled data, but differences in surface armouring also have a large impact.

Variable	Coefficient	Standard Error	t	p-value	VIF ¹
Intercept	2.991×10^{-5}	0.077	-135.680	0.000	
Q/Q_d	1.671	0.035	45.156	0.000	1.099
D_{84}^*	-2.371	0.063	-37.520	0.000	1.565
BR	0.809	0.264	3.067	0.002	1.257
RP	4.482	0.077	57.921	0.000	1.155
SP	1.557	0.125	12.453	0.000	1.273

Residual standard error: 2.579 on 5470 degrees of freedom

Multiple $R^2 = 0.60$; Adjusted $R^2 = 0.60$

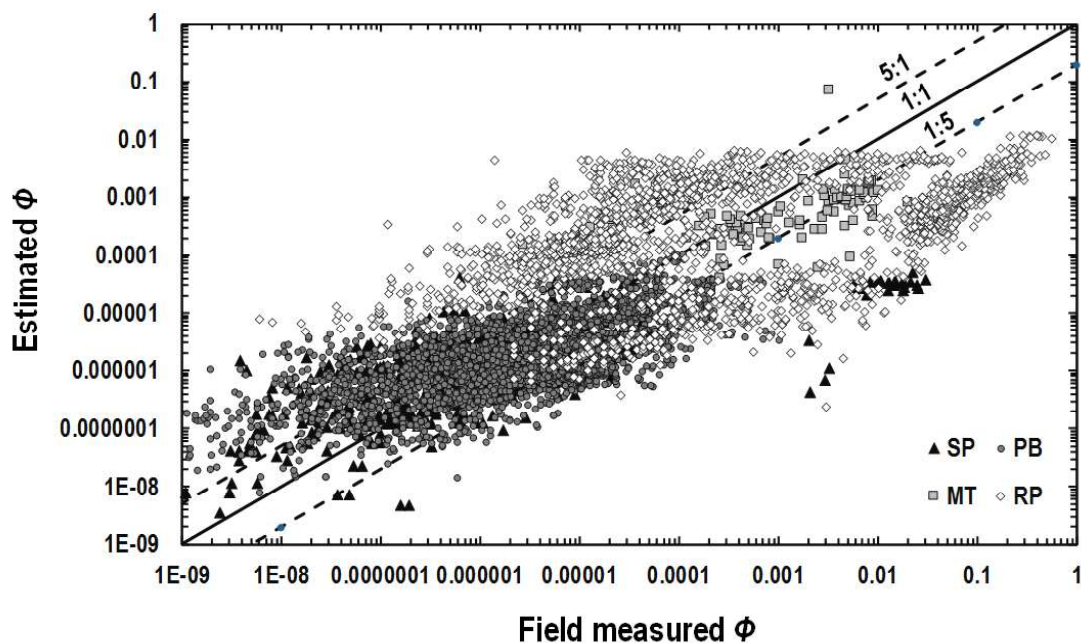
F-statistic: 1611 on 5 and 5470 degrees of freedom. $p\text{-value} = 2.2 \times 10^{-16}$

¹ Variance Inflation Factor

Table 5. Results from the multiple regression model based on eq. 8 (see main text).

449 Different channel morphologies and macro-bedforms result from the adjustment of channel
 450 macro-roughness to different balances between sediment supply and transport capacity
 451 (Montgomery and Buffington, 1997); similarly, armouring is the consequence of the adjustments
 452 in roughness at the grain-scale to the same balances between sediment supply and capacity
 453 (Dietrich et al., 1989; Venditti et al., 2017). Consequently, both dominant channel morphology
 454 and armour ratios constitute a proxy of sediment supply and should be related. Interestingly
 455 enough, we have observed systematic differences in armour ratios between the different channel
 456 morphologies (see Figure 3). In general, multi-thread channels and rivers with riffles and pools

1745
 1746
 1747 457 exhibit a lower degree of surface armouring, while plane-bed and step-pool channels show higher
 1748
 1749 458 armour ratios. Higher armour ratios in step-pool channels could be related to the existence of
 1750
 1751 459 jammed stones and large immobile boulders that may contribute to larger armour ratios. In plane
 1752
 1753 460 bed channels, large protruding grains and immobile stones defining transversal ribs and cells are
 1754
 1755 461 also common (Church et al., 1998), and may help define a surface coarser than in riffle and pool
 1756
 1757 462 and braided channels. Following this, eq. 8 would provide a mathematical expression describing
 1758
 1759 463 how the increase in bedload rates with flow discharge is modulated by the differences in sediment
 1760
 1761 464 supply, which is parameterised through the armour ratio and the dummy variables (i.e. dominant
 1762
 1763 465 macro-bedforms). In Figure 12, we compare the transport intensities estimated using eq. 8 to the
 1764
 1765 466 true values measured in the field. Regression predictions plot close to the 1:1 line, with an average
 1766
 1767 467 0.9 ratio between predictions and truth-values and 43% of points showing a discrepancy lower
 1768
 1769 468 than one order of magnitude. Riffle and pool and braided data show a larger scatter than plane-
 1770
 1771 469 bed and step-pool morphologies; this is probably related to the larger cross-sectional variability
 1772
 1773 470 in shear stress and sediment paths, typical of these channel settings (Recking et al., 2016;
 1774
 1775 471 Vázquez-Tarrió et al., 2018).



1796 **Figure 12.** Bedload transport intensities estimated using eq. 8 plotted versus transport
 1797 intensities measured in the field. MT: Multi-thread channels; PB: Plane-bed; RP: Riffle and
 1798 pool; SP: step-pool streams.
 1799
 1800
 1801
 1802
 1803

1804
1805
1806 472 **5. Discussion**
1807

1808 473 **5.1. Sediment supply accommodated through armouring in gravel-bed rivers**
1809

1810 474 Our meta-analysis shows a decline in the armour ratio with increasing bedload supplies
1811
1812 475 (quantified through the q^* -metrics and q_s/ω_{dd}) in the compiled field data (Figures 7 and 8), which
1813
1814 476 is similar to the trends observed in previous flume experiments (Dietrich et al., 1989; Venditti et
1815
1816 477 al., 2017). In this regard, plots shown in Figures 7 and 8 quantify the important imprint of
1817
1818 478 sediment supply over surface armouring in gravel-bed rivers. It should be noted that q^* was
1819
1820 479 computed based on subsurface GSD, using the common approach of equalling subsurface GSD
1821
1822 480 to the average GSD of the bedload. However, bedload capacities would be more adequately
1823
1824 481 computed based on the actual GSD of the bedload. There may be situations where shifts in
1825
1826 482 sediment sources and catchment patterns of sediment production could lead to changes in the
1827
1828 483 grain size of the sediment supplies; for instance, mountain watersheds submitted to massive
1829
1830 484 afforestation (or forest clearance), or river reaches fed by largely managed (e.g. dammed,
1831
1832 485 dredged) tributaries. In such situations, we would expect changes in the GSD of the bedload
1833
1834 486 (fining or coarsening) that may derive in a change in bedload transport capacities; this would in
1835
1836 487 turn influence surface GSD together with changes in the amount of sediment inputs.

1837 488 There is a certain amount of unexplained scatter within the data in Figures 7 and 8, so there should
1838
1839 489 be other contributing and explanatory variables for data variance in them apart from bedload
1840
1841 490 supply. We believe that the variability introduced by differences in the shape of the dominant
1842
1843 491 competent flow hydrograph and flow duration (Hassan et al., 2006; Phillips et al., 2018) are the
1844
1845 492 most probable candidates. These flow parameters would be largely variable amongst the selected
1846
1847 493 study reaches and could not be described by a single q^* or q_s/ω ratio based only on peak discharge.
1848
1849 494 As pointed out above, gravel-bed streams submitted to long receding hydrograph limbs and
1850
1851 495 experiencing several floods per year are likely to develop a higher degree of armouring than
1852
1853 496 equivalent streams in terms of sediment supply, but experiencing less frequent flooding and a
1854
1855 497 short falling limb (Hassan et al., 2006). Therefore, flood hydrograph may exert an important
1856
1857 498 control on armouring, together with sediment supply. Although the available data do not let us
1858
1859 499 explore this issue in much depth, in general they are in agreement with this general picture:
1860
1861
1862

1863
1864
1865
1866
1867
1868
1869
1870
1871
1872
1873
1874
1875
1876
1877
1878
1879
1880
1881
1882
1883
1884
1885
1886
1887
1888
1889
1890
1891
1892
1893
1894
1895
1896
1897
1898
1899
1900
1901
1902
1903
1904
1905
1906
1907
1908
1909
1910
1911
1912
1913
1914
1915
1916
1917
1918
1919
1920
1921

500 snowmelt-dominated data tend to show larger armour than rainfall-dominated rivers in Figure 6,
501 although the possibility of time lags between previous changes in upstream sediment inputs and
502 streambed adjustment, or even some seasonal variability in sediment supply, should not be
503 dismissed, since both may play a role in the variability documented in the compiled data. The
504 influence on armouring of these time lags and seasonal variability in sediment inputs may be more
505 important in those channel morphologies better coupled or connected with upstream sediment
506 sources (e.g. braided channels), where one-shot observations of armour ratios may not detect well
507 the average trends.

508 However, despite the scatter in the data, the overall picture shown by Figures 9 and 10 illustrates
509 how the signal linked to differences in sediment yields is the dominant one, and it is globally well-
510 recorded through the surface grain size and the armour ratio in gravel-bed rivers. Our analysis
511 suggests that sediment supply drives streambed surface GSD in gravel-bed rivers in two different
512 ways: i. the GSD of the sediment supplied and introduced into the channel network exerts an
513 obvious control, since it defines the range of grain sizes that are available in the bed material
514 (Figure 4); ii. streambed surface represents the sediment layer in more intimate contact with fluid
515 forces, so it adjusts to the balances between volumes of sediment supplied into the channel and
516 the streams' capacity to transfer these sediment inputs downstream out from the reach (Figures 9
517 and 10). In principle, stream ability to convey sediment inputs downstream is size-selective (Paola
518 and Seal, 1995), and this partially explains why the surface layer tends to coarsen. This influence
519 of hydraulic conditions could be eventually more important and partially blur the primary
520 influence of the GSD of the bedload.

521 Based on our data and quantile regression analysis, we have created two diagrams illustrating the
522 likelihood of a certain armour ratio for a given sediment supply (Figure 11). We believe these
523 diagrams provide a useful frame to interpret armour ratios measured in the field, and to
524 characterize streambed state and mobility in a quick way. For many applied issues (channel-
525 design, river restoration), an adequate diagnosis of the hydro-morphological status of a given
526 reach is fundamental. However, information of bedload fluxes is lacking in many cases. In such
527 cases, armour ratios measured in the field may provide a quick characterization of the sediment

1922
1923
1924
1925
1926
1927
1928
1929
1930
1931
1932
1933
1934
1935
1936
1937
1938
1939
1940
1941
1942
1943
1944
1945
1946
1947
1948
1949
1950
1951
1952
1953
1954
1955
1956
1957
1958
1959
1960
1961
1962
1963
1964
1965
1966
1967
1968
1969
1970
1971
1972
1973
1974
1975
1976
1977
1978
1979
1980

528 supply conditions and streambed mobility of the considered river reach, by combining diagrams
529 such as those shown in Figure 9 with some qualitative knowledge about the dominant
530 hydrological regime.

531 ***5.2. Implications for equilibrium channel geometry***

532 We observed how in most of the compiled data shear stresses at the dominant discharge are close
533 to critical thresholds for sediment motion (Figure 10). These observations reflect the streambed's
534 surface adjustment to dominant hydraulic conditions. In this respect, theoretical work (Parker,
535 1978; Parker, 1979) and decades of observations in gravel-bed alluvial channels (Parker, 2004;
536 Mueller and Pitlick, 2005; Parker et al., 2007) supported the hypothesis of threshold or near-
537 threshold channels (Parker et al., 2007; Phillips and Jerolmack, 2016; Métivier et al., 2017).
538 According to this idea, alluvial channel dimensions adjust in such a way that the threshold for the
539 motion of median-size grains occurs close to bankfull flows (e.g. MacKenzie et al., 2018).

540 However, in our data Shields values at the dominant discharge are close to the critical thresholds
541 for the entrainment of the coarser fraction of bed sediment only in well-armoured streams (Figure
542 10); otherwise, Shields stresses are well above these critical values in poorly armoured streams.
543 Pfeiffer et al. (2017) observed that only supply-limited streams meet the threshold channel
544 condition, while in capacity-limited systems they reported Shields stresses at bankfull
545 considerably over the critical levels. Based on these observations, these authors concluded that
546 the common observation of channels adjusting to threshold conditions simply reflects the fact that
547 the channels most commonly surveyed in the field are subject to modest sediment supplies.

548 Nevertheless, we propose an alternative interpretation for the trends shown in Figure 10 and
549 Pfeiffer et al. (2017). According to the data analysed in this manuscript, high-sediment supply
550 systems correspond mainly to multi-thread and riffle-pool streams (Figure 3). These kinds of
551 settings are characterized by bar morphologies, which involve complex 3D flow structures
552 (Francalanci et al., 2012), specific patterns of grain size sorting (Paola, 1989; Lisle et al., 1992)
553 and a great variability in shear stress distributions across their cross-section (Recking, 2009;
554 Recking et al., 2016). Furthermore, gravel dunes and bedload sheet propagation (Venditti et al.,
555 2017) represent an additional source of form roughness in these rivers. Consequently, we expect

1981
1982
1983
1984
1985
1986
1987
1988
1989
1990
1991
1992
1993
1994
1995
1996
1997
1998
1999
2000
2001
2002
2003
2004
2005
2006
2007
2008
2009
2010
2011
2012
2013
2014
2015
2016
2017
2018
2019
2020
2021
2022
2023
2024
2025
2026
2027
2028
2029
2030
2031
2032
2033
2034
2035
2036
2037
2038
2039

556 larger biases in bedload estimates when averaging shear stresses across the cross section of these
557 streams (Recking, 2013). Therefore, it is possible that 1D averaged shear stresses are not an
558 adequate proxy for the actual variability in shear stresses acting at the local and grain scales in
559 riffle and pool and multi-thread settings. This may explain the observed deviation from near-
560 threshold conditions, which could be to a large degree an artefact resulting from the assumptions
561 made when estimating cross-section averaged shear stresses (Yager et al., 2018).

562 ***5.3. Armour ratio: a proxy for the channel planform configuration***

563 Our review outlined differences in armour ratios according to channel morphology (Figure 3),
564 with multi-thread and riffle and pool rivers exhibiting, in general, a lower degree of surface
565 armouring than plane-bed and step-pool channels. The scale of the roughness and protruding
566 elements in step-pool channels is in general larger, with channel-spanning ribs (steps) composed
567 by an accumulation of jammed cobbles and boulders transverse or oblique to the channel
568 (Zimmermann and Church, 2001; Chin and Wohl, 2005), alternating with pools (Church and
569 Zimmermann, 2007; Lamarre and Roy, 2008). Step-pool streams are normally close to headwater
570 areas and are largely dependent on the accumulation of relatively fine colluvium inputs into pools
571 and around protruding boulders (Turowski et al., 2011; Recking, 2012; Recking et al., 2012; Piton
572 and Recking, 2017). Accordingly, protruding cobbles and boulders can be found on the bed
573 surface of step-pool channels, even with large sediment supplies and thick alluvial covers. This
574 may explain the generally larger armour ratios observed for step-pool streams. Similarly, the data
575 for braided rivers tend to show lower armour ratios (Figure 3), which results from the large
576 sediment inputs typical of braided streams.

577 The trends in armour ratios with channel morphology documented here suggest that planform
578 style, dominant macrobedforms, streambed mobility and grain size adjust together to dominant
579 sediment supply conditions. In this regard, a typical sequence of reach types observed in many
580 mountain basins corresponds to a downstream progression from step pool at headwaters, plane-
581 bed (or forced pool-riffle) to pool-riffle and/or multithreaded channel morphologies at the
582 piedmont valley (e.g. Warburton, 2007). In their seminal paper, Montgomery and Buffington
583 (1997) suggested that this kind of longitudinal sequence describes opposing trends between

2040
2041
2042 584 sediment supply and transport capacities in the downstream direction. In this regard, Pitlick et al.
2043
2044 585 (2008) documented a downstream trend to lower armour ratios in rivers from Colorado and Utah.
2045
2046 586 The trends observed here are in good agreement with this general scheme.
2047
2048 587 Additionally, gravel-bed rivers exhibit a wide diversity of bed features that are larger than
2049
2050 588 individual clasts and smaller than reach-scale patterns. Sediment supply plays a critical role in the
2051
2052 589 development of one kind of bed structuration or another (Buffington and Montgomery, 1999;
2053
2054 590 Venditti et al., 2017.). Dominant bedforms in gravel bed rivers evolve from gravel dunes (Carling,
2055
2056 591 1999) and bedload sheets in poorly armoured streams (Whiting et al., 1988; Nelson et al., 2009;
2057
2058 592 Recking et al., 2009), to a sequence of pebble clusters (Brayshaw, 1984), transverse ribs (Koster,
2059
2060 593 1978; Allen, 1984), stone lines (Laronne and Carson, 1976) and reticulate stone cells (Church et
2061
2062 594 al., 1998; Hassan and Church, 2000) with decreasing sediment supplies (Venditti et al., 2017).
2063
2064 595 Indeed, the stability of a gravel streambed is increased by the presence of particle arrangements
2065
2066 596 and clusters (e.g., Reid and Frostick, 1984; Church et al., 1998; Hassan and Church, 2000; Piedra
2067
2068 597 et al., 2012; Ockelford and Haynes, 2013; Heays et al., 2014). Therefore, streambed textures
2069
2070 598 adjust to sediment supply reductions not only through surface coarsening, but also through a
2071
2072 599 decrease in streambed mobility and a different bed surface organization. Venditti et al. (2017)
2073
2074 600 have proposed a phase diagram for bedforms in gravel bed rivers, relating q^* to the armour ratio
2075
2076 601 (Figures 16.5 and 16.9 in Venditti et al., 2017) that is in some way comparable to our Figure 7. If
2077
2078 602 armour ratio varies in parallel to channel morphology, dominant macroforms, bed sediment
2079
2080 603 mobility and streambed structures (as our analysis shows), then the armour ratio should be
2081
2082 604 considered not only as some kind of ‘textural imprint’ of sediment supply conditions, but also as
2083
2084 605 a proxy of the streambed’s organization and structuration (Venditti et al., 2017).
2085
2086 606

2087 607 **6. Concluding Remarks**

2089 608 A large body of research in fluvial geomorphology has contributed to establishing the general
2090
2091 609 idea that sediment supply, bedload fluxes, channel morphology, bankfull shear stresses and
2092
2093 610 surface grain size are intimately related in gravel bed rivers. In this paper, we aimed to quantify
2094
2095 611 the existing links between sediment supply and surface coarsening. Based on the re-analysis of a
2096
2097
2098

2099
2100
2101
2102
2103
2104
2105
2106
2107
2108
2109
2110
2111
2112
2113
2114
2115
2116
2117
2118
2119
2120
2121
2122
2123
2124
2125
2126
2127
2128
2129
2130
2131
2132
2133
2134
2135
2136
2137
2138
2139
2140
2141
2142
2143
2144
2145
2146
2147
2148
2149
2150
2151
2152
2153
2154
2155
2156
2157

612 large database of bedload discharge information for gravel-bed streams, we have proposed semi-
613 empirical relations describing how surface grain-size and armour ratios evolve with the balances
614 between bedload yields and channel sediment transport capacities. Armour ratios increase with
615 decreasing sediment inputs, as inferred from the dimensional analysis of bedload equations and
616 as already shown by previous flume experiments.

617 Accounting for armouring is important for many reasons, since it influences the local availability
618 of bedload, hydraulic roughness, bed permeability, and physical conditions for aquatic organisms.
619 We believe that the empirical relationships found here between bedload yields and armour ratios
620 have the potential to provide a quantitative frame for exploring the links between surface
621 armouring, hydraulics and sediment availability in specific gravel-bed reaches and are a step
622 towards predicting textural adjustments to changes in sediment supply (for example, downstream
623 dams). Additionally, since armouring can provide important qualitative information about the
624 bedload regime (e.g. partial mobility vs. full mobility, sediment supply) of a specific river reach,
625 our results may potentially provide some interesting clues for palaeohydrological analysis.

626

627 **Acknowledgements:** The present work has been possible thanks to the financial support provided
628 by the grant ACB17-44, co-funded by the post-doctoral ‘Clarín’ program-FICYT (Government
629 of the Principality of Asturias) and the Marie Curie Co-Fund. This work was also performed
630 within the framework of the EUR H2O’Lyon (ANR-17-EURE-0018) of Université de Lyon
631 (UdL), within the program ‘Investissements d’Avenir’ operated by the French National Research
632 Agency (ANR). We would like to thank Pablo Turrero García and Daniel Grace for their review
633 of the English version of the manuscript.

2158
2159
2160
2161
2162
2163
2164
2165
2166
2167
2168
2169
2170
2171
2172
2173
2174
2175
2176
2177
2178
2179
2180
2181
2182
2183
2184
2185
2186
2187
2188
2189
2190
2191
2192
2193
2194
2195
2196
2197
2198
2199
2200
2201
2202
2203
2204
2205
2206
2207
2208
2209
2210
2211
2212
2213
2214
2215
2216

Notations

D :	Grain-size (particle diameter)
D_{is} :	i -th percentile of the surface grain-size distribution
D_{iss} :	i -th percentile of the subsurface grain-size distribution
D_i^* :	Armour ratio, or the ratio between the i -th percentiles of the surface and subsurface grain-size distributions
D_i^{**} :	Corrected version of the armour ratio, i.e. armour ratio computed accounting for the inherent covariation between surface and subsurface grain sizes
f :	Ratio between the armour ratio estimated based on the 84-th percentiles (D_{84}) and the armour ratio based on the median size (D50) of the grain size distribution
GSD:	Grain size distribution
ϕ :	Bedload transport intensity (Einstein parameter)
q_s :	Bedload transport rate per unit width
q_{ss} :	Channel's bedload transport capacity (per unit width) to mobilize the subarmour sediment
q_{sss} :	Channel's bedload transport capacity (per unit width) to mobilize the subarmour sediment
q^* :	Bedload 'supply index', or the ratio between q_{ss} and q_{sss}
Q :	Peak discharge
Q_d :	Peak discharge for the dominant discharge
Q/Q_d :	Flow ratio
ω :	Specific streampower
τ :	Section-averaged bed shear stress
τ^* :	Dimensionless (section-averaged) Shields shear stress
τ_c :	Critical (section averaged) bed shear stress for sediment entrainment
τ_{cs} :	Critical (section averaged) bed shear stress for the inception of motion of the surface sediment particles
τ_{css} :	Critical (section averaged) bed shear stress for the inception of motion of the subsurface sediment particles
τ_{ci}^* :	Critical threshold Shields stress for entrainment particle with sizes corresponding to the i -th percentile of the grain-size distribution

2217
2218
2219
2220
2221
2222
2223
2224
2225
2226
2227
2228
2229
2230
2231
2232
2233
2234
2235
2236
2237
2238
2239
2240
2241
2242
2243
2244
2245
2246
2247
2248
2249
2250
2251
2252
2253
2254
2255
2256
2257
2258
2259
2260
2261
2262
2263
2264
2265
2266
2267
2268
2269
2270
2271
2272
2273
2274
2275

662 **References**

663 Allen, J. R. L. (1984). *Sedimentary Structures, Their Character and Physical Basis*. Elsevier,
664 Amsterdam.

665 Almedeij, J. H. (2002). *Bedload transport in gravel- bed streams under a wide range of Shields*
666 *stresses*. Ph.D. thesis, Va. Polytech. Inst. and State Univ., Blacksburg.

667 Andrews, E. D. (1994). Marginal bed load transport in a gravel bed stream, Sagehen Creek,
668 California. *Water Resources Research*, 30, 2241–2250.

669 Andrews, E. D. and Erman, D. C. (1986). Persistence in the size distribution of surficial bed
670 material during an extreme snowmelt flood. *Water Resources Research*, 22, 191–197.

671 Andrews, E.D. and Parker, G. (1987): Formation of a coarse surface layer as the response to
672 gravel mobility. In: Thorne, C.R., Bathurst, J.C. and Hey, R.D. (eds). *Sediment transport*
673 *in gravel-bed rivers*, pp. 269-300. Chichester: Wiley.

674 Bacchi, V., Recking, A., Eckert, N., Frey, P., Piton, G. and Naaim, M. (2014). The effects of
675 kinetic sorting on sediment mobility on steep slopes. *Earth Surface Processes and*
676 *Landforms*, 39, 1075–1086.

677 Barry, J. J., Buffington, J. M. and King, J. G. (2004). A general power equation for predicting
678 bedload transport rates in gravel bed rivers. *Water Resources Research*, 40, W104001.

679 Berni, C., Perret, E. and Camenen, B. (2018). Characteristic time of sediment transport decrease
680 in static armour formation. *Geomorphology*, 317, 1-9.

681 Bertin, S. and Friedrich, H. (2018). Effects of surface texture and structure on the development
682 of stable fluvial armors. *Geomorphology*, 306, 64-79.

683 Borland, W. M. (1960). *Stream Channel Stability*. U.S. Bureau of Reclamation, Denver.

684 Brasington, J., Vericat, D. and Rychov, I. (2012). Modeling river bed morphology, roughness,
685 and surface sedimentology using high resolution terrestrial laser scanning. *Water*
686 *Resources Research*, 48 (2012), Article W11519.

687 Brayshaw, A. C. (1984). Characteristics and origin of cluster bedforms in coarse-grained alluvial
688 channels. *Sedimentology of Gravels and Conglomerates*, 10, 77-85.

689 Buffington, J. M. (2012). Changes in channel morphology over human time scales. In: Church,
690 M., Biron, P.M., Roy, A.G. (eds.), *Gravel-bed Rivers: Processes, Tools, Environments*,
691 chapter 32, pp. 435–463. Wiley, Chichester, UK.

692 Buffington, J. M. and Montgomery, D. R. (1999). A procedure for classifying textural facies in
693 gravel-bed rivers. *Water Resources Research*, 35 (6), 1903-1914.

2276
2277
2278
2279
2280
2281
2282
2283
2284
2285
2286
2287
2288
2289
2290
2291
2292
2293
2294
2295
2296
2297
2298
2299
2300
2301
2302
2303
2304
2305
2306
2307
2308
2309
2310
2311
2312
2313
2314
2315
2316
2317
2318
2319
2320
2321
2322
2323
2324
2325
2326
2327
2328
2329
2330
2331
2332
2333
2334

694 Bunte, K. and Abt, S. R. (2001). *Sampling surface and subsurface particle-size distributions in*
695 *wadable gravel-and cobble-bed streams for analyses in sediment transport, hydraulics,*
696 *and streambed monitoring*. Gen. Tech. Rep. RMRS-GTR-74. Fort Collins,CO: U.S.
697 Department of Agriculture, Forest Service, Rocky Mountain Research Station. 428 p.

698 Buscombe, D. (2008). Estimation of grain size distributions and associated parameters from
699 digital images of sediment. *Sedimentary Geology*, 210, 1-10.

700 Butler, J. B., Lane, S. N. and Chandler, J. H. (2001). Automated extraction of grain-size data for
701 gravel surfaces using digital image processing. *Journal of Hydraulic Research*, 39, 519-
702 529.

703 Camenen, B., Holubová. K., Lukac, M., Le Coz, J. and Paquier, A. (2011). Assessment of
704 Methods Used in 1D Models for Computing Bed-Load Transport in a Large River: The
705 Danube River in Slovakia. *Journal of Hydraulic Engineering*, 137 (10).

706 Carling, P. A. (1999). Subaqueous gravel dunes. *Journal of Sedimentary Research*, 69, 534– 545.

707 Chin, C. O., Melville, B. W. and Raudkivi, A. J. (1994). Streambed armouring. *Journal of*
708 *Hydraulic Engineering*, 120 (8).

709 Chin, A. and Wohl, E. (2005). Toward a theory for step pool in stream channels. *Progress in*
710 *Physical Geography*, 29, 275– 296.

711 Church, M. (2006). Bed material transport and the morphology of alluvial river channels. *Annual*
712 *Review of Earth and Planetary Sciences*, 34 (1), 325-354.

713 Church, M. and Hassan, M. A. (2002). Mobility of bed material in Harris Creek. *Water Resources*
714 *Research*, 38 (11), 1237.

715 Church, M. and Hassan, M. (2005). Upland gravel-bed rivers with low sediment transport. In:
716 Garcia, C. and Batalla, R.J. (eds). *Catchment Dynamics and River Processes.*
717 *Mediterranean and Other Climate Regions*. Developments in Earth Surface Processes 7,
718 pp. 141-168, Amsterdam, Elsevier.

719 Church, M., Hassan, M. A. and Wolcott, J. F. (1998). Stabilizing self- organized structures in
720 gravel- bed stream channels: Field and experimental observations. *Water Resources*
721 *Research*, 34 (11), 3169– 3179.

722 Church, M. A., McLean, D. G. and Wolcott, J. F. (1987). River Bed Gravels: Sampling and
723 Analysis. In: Thorne, C. R., Bathurst, J. C. and Hey, R. D. (eds). *Sediments transport in*
724 *Gravel Bed Rivers*, pp. 43-88. John Wiley and Sons, New York.

725 Church, M. and Rood, K. (1983). *Catalogue of alluvial river channel regime data*, Dep. of
726 Geography, Univ. of British Columbia, Vancouver.

2335
2336
2337 727 Church, M. and Zimmermann, A. (2007). Form and stability of step- pool channels: research
2338 progress. *Water Resources Research*, 43, W03415.
2339 728
2340
2341 729 Clayton, J. A. and Pitlick, J. (2008). Persistence of the surface texture of a gravel-bed river during
2342 a large flood. *Earth Surface Processes and Landforms*, 33, 661–673.
2343 730
2344 731 Cui, Y., Parker, G., Lisle, T. E., Gott, J., Hansler- Ball, M. E., Pizzuto, J. E., Allmendinger, N.
2345 E., and Reed, J. M. (2003). Sediment pulses in mountain rivers: 1. Experiments. *Water*
2346 *Resources Research*, 39, 1239,
2347 732
2348 733
2349 734 Curran, J. and Waters, K. A. (2014). The importance of bed sediment sand content for the structure
2350 of a static armor layer in a gravel bed river. *Journal of Geophysical Research: Earth*
2351 *Surface*, 119, 1484–1497.
2352 736
2353
2354 737 Dietrich, W., Kirchner, J., Ikeda, H., and Iseya, F. (1989). Sediment supply and the development
2355 of the coarse surface layer in gravel-bedded rivers. *Nature*, 340, 215–217.
2356 738
2357
2358 739 Emmett, W. W. and H. R. Seitz (1974). *Suspended- and bedload- sediment transport in the Snake*
2359 *and Clearwater rivers in the vicinity of Lewiston, Idaho (July 1973 through July 1974)*.
2360 U.S. Geological Survey, Boise, Idaho.
2361 741
2362 742 Erwin, S. O., Schmidt, J. C. and Nelson, N. C. (2011). Downstream effects of impounding a
2363 natural lake: the Snake River downstream from Jackson Lake Dam, Wyoming, USA.
2364 *Earth Surface Processes and Landforms*, 36, 1421-1434.
2365 744
2366
2367 745 Ferdowsi, B., Ortiz, C.P., Houssais, M. and Jerolmack, D.J. (2017). River-bed armouring as a
2368 granular segregation phenomenon. *Nature Communications*, 8, 1363.
2369 746
2370
2371 747 Ferguson, R.I. (2003). The missing dimension: effects of lateral variation on 1-D calculations of
2372 fluvial bedload transport. *Geomorphology*, 56, 1-14.
2373 748
2374 749 Ferguson, R. (2007). Flow resistance equations for gravel and boulder bed streams. *Water*
2375 *Resources Research*, 43, W05427, 1– 12.
2376 750
2377
2378 751 Ferguson, R., and Church, M. (2009). A critical perspective on 1-D modeling of river processes:
2379 gravel load and aggradation in lower Fraser River. *Water Resources Research*, 45,
2380 W11424
2381 753
2382
2383 754 Francalanci, S., Solari, L., Toffolon, M. and Parker G. (2012). Do alternate bars affect sediment
2384 transport and flow resistance in gravel- bed rivers? *Earth Surface Processes and*
2385 *Landforms*, 37 (8), 866– 875.
2386 756
2387
2388
2389
2390
2391
2392
2393

2394
2395
2396
2397
2398
2399
2400
2401
2402
2403
2404
2405
2406
2407
2408
2409
2410
2411
2412
2413
2414
2415
2416
2417
2418
2419
2420
2421
2422
2423
2424
2425
2426
2427
2428
2429
2430
2431
2432
2433
2434
2435
2436
2437
2438
2439
2440
2441
2442
2443
2444
2445
2446
2447
2448
2449
2450
2451
2452

757 Gessler, J., (1967). *The Beginning of Bedload Movement of Mixtures Investigated as Natural*
758 *Armoring in Channels*. W.M. Keck Laboratory of Hydraulics and Water Resources,
759 California Institute of Technology, Pasadena, Translation T-5.

760 Gessler, J. (1970). Self- stabilizing tendencies of alluvial channels. *Journal of the Waterways,*
761 *Harbors and Coastal Engineering Division, American Society of Civil Engineers*, 96 (2),
762 235– 249, 1970.

763 Gomez, B. (1983). Temporal variations in bedload transport rates: the effect of progressive bed
764 armouring. *Earth Surface Processes and Landforms*, 8 (1), 41–54.

765 Gomez, B. (1988). *Two data sets describing channel- wide temporal variations in bedload-*
766 *transport rates*. U.S. Geological Survey. Public Data File, 88- 88, 26 pp.

767 Gomez, B. (1993). Roughness of stable, armored gravel beds. *Water Resources Research*, 29 (11),
768 3631–3642.

769 Gomez, B. (1994). Effects of particle shape and mobility on stable armor development. *Water*
770 *Resources Research*, 30 (7), 2229–2239.

771 Graham, D. J., Reid, I. and Rice, S. P. (2005). Automated sizing of coarse-grained sediments:
772 image-processing procedures. *Mathematical Geology*, 37, 1-28.

773 Harrison, H. S. (1950). *Report on special investigations of bed sediment segregation in a*
774 *degrading bed*. Inst. of Eng. Res., University of California, Berkeley.

775 Haschenburger, J.K. and Wilcock, P.R. (2003). Partial transport in a natural gravel bed channel.
776 *Water Resources Research*, 39 (1), 1020.

777 Haschenburger, J. K. (2017) Streambed Disturbance over a Long Flood Series. *River Research*
778 *and Applications*, 33: 753– 765.

779 Hassan, M. A. and M. Church (2000). Experiments on surface structure and partial sediment
780 transport. *Water Resources Research*, 36, 1885 – 1895.

781 Hassan, M. A., Egozi, R. and Parker, G. (2006). Experiments on the effect of hydrograph
782 characteristics on vertical grain sorting in gravel bed rivers. *Water Resources Research*,
783 42, W09408.

784 Hassan, M. A. and Zimmermann, A. (2012). Channel Response and Recovery to Changes in
785 Sediment Supply. In: Church, M., Biron, P. M. and Roy, A. G. (eds). *Gravel-Bed Rivers:*
786 *Processes, Tools, Environments*, chapter 33, pp. 464-473. Wiley & Sons, Chichester, UK.

787 Heays, K. G., Friedrich, H. and Melville, B. W. (2014). Laboratory study of gravel-bed cluster
788 formation and disintegration. *Water Resources Research*, 50, 2227–2241.

2453
2454
2455
2456
2457
2458
2459
2460
2461
2462
2463
2464
2465
2466
2467
2468
2469
2470
2471
2472
2473
2474
2475
2476
2477
2478
2479
2480
2481
2482
2483
2484
2485
2486
2487
2488
2489
2490
2491
2492
2493
2494
2495
2496
2497
2498
2499
2500
2501
2502
2503
2504
2505
2506
2507
2508
2509
2510
2511

789 Heritage, G. and Milan, D. J. (2009). Terrestrial laser scanning of grain roughness in a gravel bed
790 river. *Geomorphology*, 113 (1), pp. 4-11.

791 Hinton, D., Hotchkiss, R. H. and Cope, M. (2018). Comparison of Calibrated Empirical and Semi-
792 Empirical Methods for Bedload Transport Rate Prediction in Gravel Bed Streams.
793 *Journal of Hydraulic Engineering*, 144 (7).

794 Ibbeken, H. and Schleyer, R. (1986). Photo- sieving: A method for grain- size analysis of coarse-
795 grained, unconsolidated bedding surfaces. *Earth Surface Processes and Landforms*, 11,
796 59-77.

797 Jain, S. (1990). Armor or Pavement. *Journal Hydraulic Engineering. ASCE*, 116, 436– 440.

798 Jones, M. L. and H. R. Seitz (1980). *Sediment transport in the Snake and Clearwater rivers in the*
799 *vicinity of Lewiston, Idaho*. U.S. Geological Survey. Open File Rep., 80- 690, 179 pp.

800 Kellerhals, R. and Bray, D.L. (1971). Sampling procedures for coarse fluvial sediment. *Journal*
801 *of the Hydraulic Division. ASCE*, 97. 1165-1179.

802 King, J. G., W. W. Emmett, P. J. Whiting, R. P. Kenworthy, and J. J. Barry (2004). *Sediment*
803 *transport data and related information for selected gravel-bed streams and rivers in*
804 *Idaho*. U.S. For. Serv. Gen. Tech. Rep. RM, RMRS-GTR-131, 26 pp.

805 Klaassen, G. J. (1988). Armoured river beds during flood. *Tech. Rep. 394, Delft Hydraulics,*
806 *Emmeloord, the Netherlands*.

807 Koster, E. H. (1978). Transverse ribs: their characteristics, origin, paleohydraulic significance.
808 In: Miall, A. D. (ed). *Fluvial Sedimentology*, pp. 161-186. Canadian Society of Petroleum
809 Geologists. Mem. 5.

810 Kuhnle, R. A. (1992). Fractional transport rates of bedload on Goodwin Creek. In: Billi, P. (ed).
811 *Dynamics of Gravel Bed Rivers*, pp. 141–155, John Wiley, New York.

812 Kuhnle, R.A. and Willis, J. C. (1992). Mean size distribution of bed load on Goodwin Creek.
813 *Journal of Hydraulic Engineering*, 118, 1443–1446.

814 Lamarre, H. and Roy, A. G. (2008). The role of morphology on the displacement of particles in a
815 step–pool river system. *Geomorphology*, 99, 270– 279.

816 Lane, E.W. (1955). Design of stable channels, *Transactions ASCE*, Paper no. 2776, 20, 1234-
817 1279.

818 Laronne, J.B. and Carson, M.A. (1976). Interrelationships between bed morphology and bed
819 material transport for a small, gravel-bed channel. *Sedimentology*, 23 (1), 67–85.

2512
2513
2514 820 Laronne, J. B and Reid, I. (1993). Very high rates of bedload sediment transport by ephemeral
2515 821 desert rivers. *Nature*, 366, 148-150.
2516
2517 822 Laronne, J. B., Reid, I., Yitshack, Y. and Frostick, L. E. (1994). The non-layering of gravel
2518 823 streambeds under ephemeral flood regimes. *Journal of Hydrology*, 159 (1-4), 353-363.
2519
2520 824 Lindeman, R.H., Merenda, P.F. and Gold, R.Z. (1980). *Introduction to Bivariate and Multivariate*
2521 825 *Analysis*, Scott Foresman & Co: Glenview, IL, USA.
2522
2523 826 Lisle, T. E. (1986). Stabilization of a gravel channel by large streamside obstruction and bedrock
2524 827 bends, Jacoby Creek, northwestern California. *Geological Society of American Bulletin*,
2525 828 97, 999–1011.
2526
2527 829 Lisle, T. E. (1989). Sediment transport and resulting deposition in spawning gravels, north coastal
2528 830 California. *Water Resources Research*, 25, 1303–1319.
2529
2530 831 Lisle, T.E. (1995). Particle size variations between bed load and bed material in natural gravel
2531 832 bed channels. *Water Resources Research*, 31, 1107–1118.
2532
2533 833 Lisle, T. E. and Hilton, T. (1992). The volume of fine sediment in pools: an index of sediment
2534 834 supply in gravel- bed streams. *Water Resources Bulletin*, 28 (2), 371– 383.
2535
2536 835 Lisle, T. E. and Madej, M. A. (1992). Spatial variation in armouring in a channel with high
2537 836 sediment supply. In: Billi, P., Hey, R. D., Thorne, C.R. and Tacconi, P. (ed). *Dynamics*
2538 837 *of Gravel-bed Rivers*, pp. 277-293, John Wiley and Sons.
2539
2540 838 Little, W. C., and Mayer, P. G. (1972). *The role of sediment gradation of channel armorings*. Publ.
2541 839 ERC- 0672, 104 pp., Ga. Inst. of Technol.
2542
2543 840 MacKenzie, L. G., Eaton, B. C. and Church, M. (2018). Breaking from the average: Why large
2544 841 grains matter in gravel- bed streams. *Earth Surface Processes and Landforms*, 43, 3190–
2545 842 3196.
2546
2547 843 Madej, M. A. and V. Ozaki (1996). Channel response to sediment wave propagation and
2548 844 movement, Redwood Creek, California, USA. *Earth Surface Processes and Landforms*,
2549 845 21, 911 – 927.
2550
2551 846 Mao, L. (2012). The effect of hydrographs on bed load transport and bed sediment spatial
2552 847 arrangement. *Journal of Geophysical Research: Earth Surface*, 117 (F3).
2553
2554 848 Mao, L., Cooper, J. R., and Frostick, L. E. (2011). Grain size and topographical differences
2555 849 between static and mobile armour layers. *Earth Surface Processes and Landforms*, 36,
2556 850 1321–1334.
2557
2558
2559
2560
2561
2562
2563
2564
2565
2566
2567
2568
2569
2570

2571
2572
2573
2574
2575
2576
2577
2578
2579
2580
2581
2582
2583
2584
2585
2586
2587
2588
2589
2590
2591
2592
2593
2594
2595
2596
2597
2598
2599
2600
2601
2602
2603
2604
2605
2606
2607
2608
2609
2610
2611
2612
2613
2614
2615
2616
2617
2618
2619
2620
2621
2622
2623
2624
2625
2626
2627
2628
2629

851 Marion, A. and Fraccarollo, L. (1997). Experimental investigation of mobile armoring
852 development. *Water Resources Research*, 33, 1447–1453.

853 McLean, D. G., Church, M. and Tassone, B. (1999). Sediment transport along lower Fraser River:
854 1. Measurements and hydraulic computations. *Water Resources Research*, 35, 2533–
855 2548.

856 Marion, A., Tait, S.J. and McEwan, I.K. (2003). Analysis of small-scale gravel bed topography
857 during armoring. *Water Resources Research*, 39 (12).

858 Métivier, F. and Barrier, L. (2012). Alluvial landscape evolution: what do we know about
859 metamorphosis of gravel bed meandering and braided streams? In: Church, M., Biron, P.,
860 and Roy, A. (eds). *Gravel-bed Rivers: processes, tools, environments*, chapter 34, 474-
861 501. Wiley & Sons, Chichester.

862 Métivier, F., Lajeunesse, E. and Devauchelle, O. (2017). Laboratory rivers: Lacey’s law,
863 threshold theory, and channel stability. *Earth Surface Dynamics*, 5, 187–198.

864 Meyer-Peter, E. and Muller, R. (1948). Formulas for Bed Load Transport. *Proceedings of 2nd*
865 *meeting of the International Association for Hydraulic Structures Research*, Delft, 7 June
866 1948, 39-64.

867 Milhous, R. T. (1973). *Sediment transport in a gravel- bottomed stream*. Ph.D. thesis, Oregon
868 State University, Corvallis.

869 Misset, C., Recking, A., Legout, C., Bakker, M., Bodereau, N., Borgniet, L., Cassel, M., Geay,
870 T., Gimbert, F., Navratil, O., Piegay, H., Valsangkar, N., Cazilhac, M., Poirel, A. and
871 Zanker, S. (in press). Combining multi-physical measurements to quantify bedload
872 transport and morphodynamic interactions in an alpine braiding river reach.
873 *Geomorphology*.

874 Montgomery, D.R. and Buffington, J.M. (1997). Channel-reach morphology in mountain
875 drainage basins. *Geological Society of America Bulletin*, 109, 596–611.

876 Moog, D. B. and Whiting, P. J. (1998). Annual hysteresis in bed load rating curves. *Water*
877 *Resources Research*, 34 (9), 2393– 2399.

878 Mueller, E. R. and Pitlick, J. (2005). Morphologically based model of bed load transport capacity
879 in a headwater stream. *Journal of Geophysical Research*, 110, F02016.

880 Mueller, E. R. and Pitlick, J. (2014). Sediment supply and channel morphology in mountain river
881 systems: 2. Single thread to braided transitions. *Journal of Geophysical Research: Earth*
882 *Surface*, 119, 1516– 1541.

2630
2631
2632
2633
2634
2635
2636
2637
2638
2639
2640
2641
2642
2643
2644
2645
2646
2647
2648
2649
2650
2651
2652
2653
2654
2655
2656
2657
2658
2659
2660
2661
2662
2663
2664
2665
2666
2667
2668
2669
2670
2671
2672
2673
2674
2675
2676
2677
2678
2679
2680
2681
2682
2683
2684
2685
2686
2687
2688

883 Mueller, E. R., Pitlick, J. and Nelson, J. M. (2005). Variation in the reference Shields stress for
884 bed load transport in gravel- bed streams and rivers. *Water Resources Research*, 41,
885 W04006.

886 Muskatirovic, J. (2008). Analysis of bedload transport characteristics of Idaho streams and rivers.
887 *Earth Surface Processes and Landforms*, 33, 1757–1768.

888 Nelson, P. A., Dietrich, W. E. and Venditti, J. G. (2010). Bed topography and the development of
889 forced bed surface patches. *Journal of Geophysical Research*, 115.

890 Nelson, P. A., Venditti, J. G., Dietrich, W. E., Kirchner, J. W., Ikeda, H., Iseya, F., and Sklar, L.
891 S. (2009), Response of bed surface patchiness to reductions in sediment supply. *Journal*
892 *of Geophysical Research*, 114, F02005.

893 Ockelford A. and Haynes, H. (2013). The impact of stress history on bed structure. *Earth Surface*
894 *Processes and Landforms*, 38 (7), 717– 727.

895 Orrú, C., Blom, A. and Uijttewaal W.S. J. (2016). Armor breakup and reformation in a
896 degradational laboratory experiment. *Earth Surface Dynamics*, 4, 461-470.

897 Paola, C. (1989). Topographic sorting. *Eos. Transactions American Geophysical Union*, 70, 332.

898 Parker, G. (1978). Self- formed rivers with equilibrium banks and mobile bed: Part II. The gravel
899 river. *Journal of Fluid Mechanics*, 89 (1), 127– 148, 1978.

900 Parker, G. (1979). Hydraulic geometry of active gravel rivers. *Journal of the Hydraulics Division.*
901 *American Society of Civil Engineers*, 105 (HY9), 1185– 1201, 1979.

902 Parker, G. (2004). *1D Sediment Transport Morphodynamics with Applications to Rivers and*
903 *Turbidity Currents*. Copyrighted ebook, available at:
904 http://hydrolab.illinois.edu/people/parkerg//morphodynamics_e-book.htm.

905 Parker, G. (2008). Transport of Gravel and Sediment Mixtures. In: García, M. (ed). *Sedimentation*
906 *Engineering: Processes, Measurements, Modeling, and Practice*. Manual and Reports in
907 Engineering Practice No. 110, American Society of Civil Engineers: Reston, VA, 165-
908 264.

909 Parker, G. and Klingeman, P.C. (1982). On why gravel bed streams are paved. *Water Resources*
910 *Research*, 18 (5), 1409–1423.

911 Parker, G., Klingeman, P.C. and McLean, D.C. (1982). Bedload and size distribution in paved,
912 gravel-bed streams. *Proceedings of the American Society of Civil Engineers, Journal of*
913 *the Hydraulics Division*, 108, 544-571.

2689
2690
2691
2692
2693
2694
2695
2696
2697
2698
2699
2700
2701
2702
2703
2704
2705
2706
2707
2708
2709
2710
2711
2712
2713
2714
2715
2716
2717
2718
2719
2720
2721
2722
2723
2724
2725
2726
2727
2728
2729
2730
2731
2732
2733
2734
2735
2736
2737
2738
2739
2740
2741
2742
2743
2744
2745
2746
2747

914 Parker, G. and Sutherland, A.J. (1990). Fluvial armor. *Journal of Hydraulic Research*, 28 (5),
915 529–544.

916 Parker, G., and C. M. Toro-Escobar (2002). Equal mobility of gravel in streams: The remains of
917 the day. *Water Resources Research*, 38(11), 1264.

918 Parker, G., Wilcock, P. R., Paola, C., Dietrich, W. E. and Pitlick, J. (2007). Physical basis for
919 quasi- universal relations describing bankfull hydraulic geometry of single- thread gravel
920 bed rivers. *Journal of Geophysical Research*, 112, F04005.

921 Pfeiffer, A. M. and Finnegan, N. J. (2018). Regional variation in gravel riverbed mobility,
922 controlled by hydrologic regime and sediment supply. *Geophysical Research Letters*, 45,
923 3097– 3106.

924 Pfeiffer, A. M., Finnegan, N. J. and Willenbring, J. K. (2017). Sediment supply controls gravel
925 river geometry. *Proceedings of the National Academy of Sciences*, 114 (13), 3346-3351.

926 Phillips, C. B., Hill, K. M., Paola, C., Singer, M. B. and Jerolmack, D. J. (2018). Effect of flood
927 hydrograph duration, magnitude, and shape on bed load transport dynamics. *Geophysical
928 Research Letters*, 45, 8264– 8271.

929 Phillips, C. B. and Jerolmack, D. J. (2016). Self-organization of river channels as a critical filter
930 on climate signals. *Science*, 352 (6286), 694-697.

931 Piedra, M. M., Haynes, H. and Hoey, T. B. (2012). The spatial distribution of coarse surface
932 grains and the stability of gravel river beds. *Sedimentology*, 59, 1014–1029.

933 Pitlick, J., Mueller, E. R. and Segura, C. (2012). Differences in sediment supply to braided and
934 single- thread channels: what do the data tell us? In: Church, M., Biron, P. M. and Roy,
935 A. G. (eds). *Gravel- Bed Rivers: Processes, Tools, Environments*, chapter 35, pp. 502-
936 511. Wiley & sons, Chichester, U. K.

937 Pitlick, J., Mueller, E. R., Segura, C., Cress, R. and Torizzo, M. (2008). Relation between flow,
938 surface layer armoring and sediment transport in gravel bed rivers. *Earth Surface
939 Processes and Landforms*, 33, 1192–1209.

940 Piton, G. and Recking, A. (2017). The concept of travelling bedload and its consequences for
941 bedload computation in mountain streams. *Earth Surface Processes and Landforms*, 42,
942 1505– 1519.

943 Powell, D. M., Reid, I. and Laronne, J. B. (2001). Evolution of bed load grain size distribution
944 with increasing flow strength and the effect of flow duration on the caliber of bed load
945 sediment yield in ephemeral gravel bed rivers. *Water Resources Research*, 37 (5), 1463–
946 1474.

2748
2749
2750 947 Powell, D. M., Ockelford, A., Rice, S. P., Hillier, J. K., Nguyen, T., Reid, I., Tate, N. J. and
2751 948 Ackerley, D. (2016). Structural properties of mobile armors formed at different flow
2752 949 strengths in gravel- bed rivers. *Journal of Geophysical Research: Earth Surface*, 121,
2753 950 1494– 1515.
2754
2755
2756 951 Proffitt, G. T. and Sutherland, A. J. (1983). Transport of non uniform sediments. *Journal of*
2757 952 *Hydraulic Research*, 21(1), 33-43.
2758
2759
2760 953 Recking, A. (2010). A comparison between flume and field bed load transport data and
2761 954 consequences for surface based bed load transport prediction. *Water Resources Research*,
2762 955 46, W03518.
2763
2764
2765 956 Recking, A. (2012). Influence of sediment supply on mountain streams bedload transport.
2766 957 *Geomorphology*, 175-176, 139-150.
2767
2768 958 Recking, A. (2013a). An analysis of nonlinearity effects on bed load transport prediction. *Journal*
2769 959 *of Geophysical Research: Earth Surface*, 118, 1264– 1281.
2770
2771 960 Recking, A. (2013b). Simple method for calculating reach-averaged bed-load transport. *Journal*
2772 961 *of Hydraulic Engineering*, 139 (1), 70–75.
2773
2774
2775 962 Recking, A. (2016). A generalized threshold model for computing bed load grain size distribution.
2776 963 *Water Resources Research*, 52, 9274– 9289.
2777
2778 964 Recking, A., Leduc, P., Liébault, F. and Church, M. (2012). A field investigation of the influence
2779 965 of sediment supply on step- pool morphology and stability. *Geomorphology*, 139–140,
2780 966 53– 66.
2781
2782
2783 967 Recking, A., Piton, G., Vázquez- Tarrío, D. and Parker, G. (2016). Quantifying the morphological
2784 968 print of bedload transport. *Earth Surface Processes and Landforms*, 41(6), 809– 822.
2785
2786
2787 969 Reid, I. and Frostick, L. E. (1984). Particle interaction and its effect on the thresholds of initial
2788 970 and final bedload motion in coarse alluvial channels. In: Koster, E. H. and Steel, R. J.
2789 971 (eds). *Sedimentology of Gravels and Conglomerates*, pp. 61-68. Canadian Society of
2790 972 Petroleum Geologists. Memoir 10.
2791
2792
2793 973 Reid, I. and Frostick, L. E. (1986). Dynamics of bedload transport in Turkey Brook, a coarse-
2794 974 grained alluvial channel. *Earth Surface Processes and Landforms*, 11, 143– 155.
2795
2796
2797 975 Reid, I. and Laronne, J. B. (1995). Bedload sediment transport in an ephemeral stream and a
2798 976 comparison with seasonal and perennial counterparts. *Water Resources Research*, 31,
2799 977 773-781.
2800
2801
2802
2803
2804
2805
2806

2807
2808
2809 978 Reid, I., Laronne, J. B. and Powell, D. M. (1995). The Nahal Yatir bedload database: Sediment
2810
2811 979 dynamics in a gravel- bed ephemeral stream. *Earth Surface Processes and Landforms*,
2812 980 20, 845–857.
2813
2814 981 Rice, S. P. and Haschenburger, J. K. (2004). A hybrid method for size characterization of coarse
2815 982 subsurface fluvial sediments. *Earth Surface Processes and Landforms*, 29, 373-389.
2817
2818 983 Richards, K. and Clifford, N. (1991). Fluvial geomorphology: structured beds in gravelly rivers.
2819 984 *Progress in Physical Geography*, 15 (4), 407-411.
2820
2821 985 Rickenmann, D. and Recking, A. (2011). Evaluation of flow resistance in gravel- bed rivers
2822 986 through a large field data set. *Water Resources Research*, 47, W07538.
2824
2825 987 Rollet, A. J., Piégay, H., Dufour, S., Bornette, G., and Persat, H. (2014). Assessment of
2826 988 consequences of sediment deficit on a gravel river bed downstream of dams in restoration
2827 989 perspectives: application of a multicriteria, hierarchical and spatially explicit diagnosis.
2829 990 *River Research and Applications*, 30, 939– 953.
2830
2831 991 Ryan, S. E. and Emmett, W. W. (2002). *The nature of flow and sediment movement in Little*
2832 992 *Granite Creek near Bondurant, Wyoming*. Gen. Tech. Rep. RMRS-GTR-90. Ogden, UT.
2833 993 U.S. Department of Agriculture, Forest Service, Rocky Mountain Research Station. 48 p.
2835
2836 994 Ryan, S. E., Porth, L. S. and Troendle C. A. (2002). Defining phases of bedload transport using
2837 995 piecewise regression. *Earth Surface Processes and Landforms*, 27, 971–990.
2838
2839 996 Ryan, S. E., Porth, L. S. and Troendle, C. A. (2005). Coarse sediment transport in mountain
2840 997 streams in Colorado and Wyoming, USA. *Earth Surface Processes and Landforms*, 30,
2842 998 269–288.
2843
2844 999 Rubin, D. M. (2004). A simple autocorrelation algorithm for determining grain size from digital
2845 1000 images of sediment. *Journal of Sedimentary Research*, 74 (1), 160-165.
2847
2848 1001 Segura, C., and Pitlick, J. (2015). Coupling fluvial- hydraulic models to predict gravel transport
2849 1002 in spatially variable flows. *Journal of Geophysical Research: Earth Surface*, 120, 834–
2850 1003 855.
2852
2853 1004 Seitz, H. R. (1977). *Suspended- and bedload- sediment transport in the Snake and Clearwater*
2854 1005 *rivers in the vicinity of Lewiston, Idaho (August 1975 through July 1976)*. Boise, Idaho,
2856 1006 U.S. Geological Survey, Open File Rep., 76- 886, 77 pp.
2857
2858 1007 Sklar, L. S., Fadde, J., Venditti, J. G., Nelson, P., Wydzyga, M. A., Cui, Y. and Dietrich, W. E.
2859 1008 (2009). Translation and dispersion of sediment pulses in flume experiments simulating
2860 1009 gravel augmentation below dams. *Water Resources Research*, 45, W08439.
2862
2863
2864
2865

2866
2867
2868 1010 Spiller, S., Rüther, N. and Baumann, B. (2012). Artificial reproduction of the surface structure in
2869 a gravel bed. *2nd IAHR Europe Congress*. TU München, Germany.
2870 1011
2871 1012 Turowski, J. M., Badoux, A. and Rickenmann, D. (2011). Start and end of bedload transport in
2872 gravel- bed streams. *Geophysical Research Letters*, 38, L04401.
2873 1013
2874
2875 1014 Vázquez-Tarrío, D., Borgniet, L., Liébault, F. and Recking, A. (2017). Using UAS optical
2876 imagery and SfM photogrammetry to characterize the surface grain size of gravel bars in
2877 a braided river (Vénéon River, French Alps). *Geomorphology*, 285, 94-105.
2878 1016
2879
2880 1017 Vázquez- Tarrío, D. and Menéndez- Duarte, R. (2015). Assessment of bedload equations using
2881 data obtained with tracers in two coarse- bed mountain streams (Narcea River basin, NW
2882 Spain). *Geomorphology*, 238, 78– 93.
2883 1019
2884
2885 1020 Vázquez-Tarrío, D. and Batalla, R. J. (2019). Assessing Controls on the Displacement of Tracers
2886 in Gravel-Bed Rivers. *Water*, 11(8), 1598.
2887 1021
2888
2889 1022 Vázquez- Tarrío, D., Recking, A., Liébault, F., Tal, M. and Menéndez- Duarte, R. (2019). Particle
2890 transport in gravel- bed rivers: Revisiting passive tracer data. *Earth Surface Processes*
2891 *and Landforms*, 44, 112– 128.
2892 1024
2893
2894 1025 Vázquez-Tarrío, D., Tal, M., Camenen, B. and Piégay, H. (2019). Effects of continuous
2895 embankments and successive run-of-the-river dams on bedload transport capacities along
2896 the Rhône River, France. *Science of the Total Environment*, 658, 1375-1389.
2897 1027
2898
2899 1028 Venditti, J. G., Dietrich, W. E., Nelson, P. A., Wydzga, M. A., Fadde, J. and Sklar, L. S. (2005).
2900 Can coarse surface layers in gravel- bedded rivers be mobilized by finer gravel bedload?
2901 *Eos Trans. AGU*, 86 (52), Fall Meet. Suppl., Abstract H51H- 05.
2902 1030
2903
2904 1031 Venditti, J. G., Dietrich, W. E., Nelson, P. A., Wydzga, M. A., Fadde, J. and Sklar, L. S. (2010a).
2905 Mobilization of coarse surface layers in gravel-bedded rivers by finer gravel bed load.
2906 *Water Resources Research*, 46, W07506.
2907 1033
2908
2909 1034 Venditti, J. G., Dietrich, W. E., Nelson, P. A., Wydzga, M. A., Fadde, J. and Sklar, L. S. (2010b).
2910 Effect of sediment pulse grain size on sediment transport rates and bed mobility in gravel
2911 bed rivers. *Journal of Geophysical Research: Earth surface*, 115, F03039.
2912 1036
2913
2914 1037 Venditti, J. G., P. A. Nelson, R. W. Bradley, D. Haught, and A. B. Gitto (2017). Bedforms,
2915 structures, patches, and sediment supply in gravel- bed rivers. In: Tsutsumi, D. and
2916 Laronne, J. B. (ed). *Gravel- Bed Rivers: Processes and Disasters*, chapter 16, 439– 466.
2917 1039
2918
2919 1040 Wiley & Sons, Chichester, UK.
2920
2921
2922
2923
2924

2925
2926
2927 1041 Vericat, D., Batalla, R. J. and Garcia, C. (2006). Breakup and reestablishment of the armour layer
2928 in a large gravel-bed river below dams: the lower Ebro. *Geomorphology*, 76, 122–136.
2929 1042
2930
2931 1043 Wang, T. and Liu, X. (2009). The Breakup of Armor Layer in a Gravel Bed Stream with No
2932 Sediment Supply. In: Zhang, C. and Tang, H. (ed). *Advances in Water Resources and*
2933 *Hydraulic Engineering, Proceedings of 16th IAHR-APD Congress and 3rd Symposium*
2934 1045 *of IAHR-ISHS*. Springer Berlin Heidelberg, 919–923.
2935 1046
2936
2937 1047 Warburton, J. (2007). Mountain Environments. In: Perry, C. and Taylor, K. (eds). *Environmental*
2938 1048 *Sedimentology*. Blackwell, Oxford.
2939
2940 1049 Wathen S.J., Ferguson R.I., Hoey T.B. and Werritty A (1995). Unequal mobility of sand and
2941 gravel in weakly bimodal sediment. *Water Resources Research*, 31, 2087-2096.
2942 1050
2943
2944 1051 Whiting, P. J., Dietrich, W. E., Leopold, L. B., Drake, T.G. and Shreve , R. L. (1988). Bedload
2945 1052 sheets in heterogeneous sediment. *Geology*, 16, 105-108.
2946
2947 1053 Wilcock, P. R. (2001). The flow, the bed, and the transport: interaction in flume and field. In:
2948 1054 Mosley, P. (ed). *Proceedings of the Fifth Gravel-Bed Rivers Workshop*, pp. 183-219. New
2949 1055 Zealand Hydrological Society, Wellington.
2950
2951
2952 1056 Wilcock, P. R. and Crowe, J. C. (2003). Surface-based models for mixed size sediment. *Journal*
2953 1057 *of Hydraulic Engineering*, 129 (2).
2954
2955 1058 Wilcock, P. R. and DeTemple, B. T. (2005). Persistence of armor layers in gravel-bed streams,
2956 1059 *Geophysical Research Letters*, 32, L08402.
2957
2958
2959 1060 Wilcock, P. R. and Kenworthy, S. T. (2002). A two- fraction model for the transport of
2960 1061 sand/gravel mixtures. *Water Resources Research*, 38(10), 1194.
2961
2962 1062 Wilcock, P. R. and McArdell, B.W. (1993). Surface-based fractional transport rates: Mobilization
2963 1063 thresholds and partial transport of a sand-gravel sediment. *Water Resources Research*,
2964 1064 29, 1297 – 1312.
2965
2966
2967 1065 Wilcock, P. R. and McArdell, B.W. (1997). Partial transport of a sand/gravel sediment. *Water*
2968 1066 *Resources Research*, 33, 235 – 245.
2969
2970
2971 1067 Wilcock, P., Pitlick, J. and Cui, Y. (2009). *Sediment transport primer: estimating bed-material*
2972 1068 *transport in gravel-bed rivers*. Gen. Tech. Rep. RMRS-GTR-226. Fort Collins, CO: U.S.
2973 1069 Department of Agriculture, Forest Service, Rocky Mountain Research Station. 78 p.
2974
2975 1070 Willets, B.B., Maizels, J.K. and Florence, J. (1988). The simulation of streambed armouring and
2976 1071 its consequences. *Proceedings of the Institution of Civil Engineers*, 84 (3), 615–617.
2977
2978
2979
2980
2981
2982
2983

2984
2985
2986
2987
2988
2989
2990
2991
2992
2993
2994
2995
2996
2997
2998
2999
3000
3001
3002
3003
3004
3005
3006
3007
3008
3009
3010
3011
3012
3013
3014
3015
3016
3017
3018
3019
3020
3021
3022
3023
3024
3025
3026
3027
3028
3029
3030
3031
3032
3033
3034
3035
3036
3037
3038
3039
3040
3041
3042

1072 Williams, G. P. and D. L. Rosgen (1989). *Measured total sediment loads (suspended loads and*
1073 *bedloads) for 93 United States streams*. U.S. Geological Survey. Open File Report, 89-
1074 67, 128 pp.

1075 Wolman, M. (1954). A method for sampling coarse river-bed material. *American Geophysical*
1076 *Union Transactions*, 35, 951–956, 1954.

1077 Woodget, A. S. and Austrums, R. (2017). Subaerial gravel size measurement using topographic
1078 data derived from a UAV- SfM approach. *Earth Surface Processes and Landforms*, 42
1079 (9), 1434– 1443.

1080 Yager, E., Kenworthy, M., and Monsalve, A. (2015). Taking the river inside: Fundamental
1081 advances from laboratory experiments in measuring and understanding bedload transport
1082 processes. *Geomorphology*, 244, 21–32.

1083 Yager, E. M., Venditti, J. G., Smith, H, J. and Schmeeckle, M. (2018). The trouble with shear
1084 stress. *Geomorphology*, 323, 41-50.

1085 Zimmermann, A. and Church, M. (2001). Channel morphology, gradient profiles and bed stresses
1086 during flood in a step- pool channel. *Geomorphology*, 40, 311– 327.

3043
3044
3045 **1087 Supplementary information to Vázquez-Tarrió et al. (*Textural signatures***
3046 **1088 *of sediment supply in gravel-bed rivers: re-visiting the armour ratio*)**

3048
3049 **1089 S. 1. Computing section-averaged bed shear stresses for the compiled data**

3050 1090 First, we used the available discharge information and Rickenmann and Recking's (2013) fit to
3051 1091 Ferguson's (2007) friction law to estimate average flow velocity (U):

3052
3053
3054
3055 1092
$$\frac{U}{\sqrt{g \cdot S \cdot D_{84}}} = 1.44 \cdot q_l^{*0.6} \cdot \left[1 + \left(\frac{q_l^*}{43.8} \right)^{0.82} \right]^{-0.24}$$
 Eq. S1
3056
3057
3058

3059 1093 where g is the gravitational acceleration, S is the channel slope, D_{84} the 84th percentile of the
3060 1094 surface GSD and q_l^* the dimensionless specific discharge:

3061
3062
3063 1095
$$q_l^* = \frac{ql}{\sqrt{g \cdot S \cdot D_{84}^3}}$$
 Eq. S2
3064
3065
3066

3067 1096 where q_l is the flow discharge normalized by channel width. Then, we estimated the water depth
3068 1097 (d) from:

3069
3070
3071 1098
$$d = \frac{ql}{U}$$
 Eq. S3
3072
3073
3074

3075 1099 For the hydraulic radius (R), we assumed a rectangular cross-section:

3076
3077 1100
$$R = \frac{d \cdot w}{2 \cdot d + w}$$
 Eq. S4
3078
3079
3080

3081 1101 where w is channel width. Finally, we computed the cross-section averaged basal shear stresses
3082 1102 from the hydraulic radius-slope product:

3083
3084 1103
$$\tau = \rho \cdot g \cdot R \cdot S$$
 Eq. S5
3085
3086
3087

3088
3089 **1105 S. 2. A simple model for armour ratios based on bedload formulae**

3090 1106 As explained in the main text, Dietrich et al. (1989) developed a metric (q^*) quantifying the
3091 1107 balances between the sediment supplied into a reach and its actual bedload transport capacities
3092 1108 (Dietrich et al., 1989; Montgomery and Buffington, 1997; Venditti et al., 2017):

3093
3094
3095 1109
$$q^* = \frac{q_{ss}}{q_{ssS}}$$
 Eq. S6
3096
3097
3098
3099
3100
3101

3102
 3103
 3104 1110 where q_s refers to the bedload transport rate per unit width and the subscripts s and ss to the surface
 3105
 3106 1111 and subsurface sediment, respectively. Combining eq. 1 with the Meyer-Peter and Muller's
 3107
 3108 1112 (1948) bedload transport equation, Dietrich et al. (1999) suggested:

3109
 3110
 3111 1113
$$q^* = \left[\frac{(\tau - \tau_{cs})}{(\tau - \tau_{css})} \right]^{1.5} \quad \text{Eq. S7}$$

3112
 3113
 3114 1114 where τ is the bed shear stresses and τ_c the critical stress for incipient motion. Writing shear
 3115
 3116 1115 stresses in their non-dimensional form (τ^*):

3117
 3118
 3119 1116
$$\tau^* = \frac{\tau}{(\rho_s - \rho) \cdot g \cdot D} \quad \text{Eq. S8}$$

3120
 3121
 3122
 3123 1117 Dietrich et al. (1989) finally arrived at:

3124
 3125
 3126 1118
$$q^* = \left(\frac{\frac{\tau}{\tau_{css}} \frac{D_{50s}}{D_{50ss}}}{\frac{\tau}{\tau_{css}} - 1} \right)^{1.5} \quad \text{Eq. S9}$$

3127
 3128
 3129
 3130 1119 This expression quantifies the links between surface armouring (D_{50s}/D_{50ss}) and sediment supply
 3131
 3132 1120 (q^*), based on Meyer-Peter and Müller's bedload equation. The same reasoning could be applied
 3133
 3134 1121 to any other bedload equation. In this paper, we decided to use Recking's (2013b) equation (after
 3135
 3136 1122 Recking et al., 2016), since this equation has been tested and validated against bedload discharge
 3137
 3138 1123 information from natural gravel-bed rivers (e.g. Hinton et al., 2018). Recking (2013b) proposed
 3139
 3140 1124 the following expression for bedload rates:

3141
 3142
 3143 1125
$$\phi = A \cdot \frac{\tau^{*\alpha}}{1 + \left(\frac{\tau_m^*}{\tau^*} \right)^\beta} \quad \text{Eq. S10}$$

3144
 3145
 3146
 3147 1126 where ϕ is the dimensionless transport rate, estimated using the Einstein parameter:

3148
 3149 1127
$$\phi = \frac{q_s}{\sqrt{g \cdot (s-1) \cdot D_{84}^3}} \quad \text{Eq. S11}$$

3150
 3151
 3152
 3153 1128 Coefficients A , α and β are three model parameters, for which values of 14, 2.5 and 4 were
 3154
 3155 1129 proposed, respectively (Recking, 2013b, Recking et al., 2016). τ_m^* is a mobility shear stress that

3102
 3103
 3104
 3105
 3106
 3107
 3108
 3109
 3110
 3111
 3112
 3113
 3114
 3115
 3116
 3117
 3118
 3119
 3120
 3121
 3122
 3123
 3124
 3125
 3126
 3127
 3128
 3129
 3130
 3131
 3132
 3133
 3134
 3135
 3136
 3137
 3138
 3139
 3140
 3141
 3142
 3143
 3144
 3145
 3146
 3147
 3148
 3149
 3150
 3151
 3152
 3153
 3154
 3155
 3156
 3157
 3158
 3159
 3160

3161
3162
3163 1130 allows to determine low transport conditions (with partial transport and bed clustering) apart from
3164
3165 1131 higher transport ones (Recking et al., 2016). Recking (2013b) estimates τ_m^* from:
3166

$$3167 \quad 1132 \quad \tau_m = (5 \cdot S + 0.06) \cdot \left(\frac{D_{84}}{D_{50}}\right)^{4.4\sqrt{S}-1.5} \quad \text{Eq. S12}$$

3172 1133 Eq. S10 is such that for low transport conditions ($\tau_{ref}^* \ll \tau_m^*$):

$$3173 \quad 1134 \quad \phi = A \cdot \frac{\tau_m^{*\alpha+\beta}}{\tau_m^\beta} \quad \text{Eq. S13}$$

3178 1135 and for higher transport conditions ($\tau_{ref}^* \ll \tau_m^*$):

$$3180 \quad 1136 \quad \phi = \tau_m^{*\alpha} \quad \text{Eq. S14}$$

3183 1137 We can now combine equation S6 with the expression for the Einstein parameter (eq. S11):

$$3184 \quad 1138 \quad q^* = \frac{q_{ss} - \phi_s}{q_{ss} - \phi_{ss}} \cdot \left(\frac{D_{84_{ss}}}{D_{84_s}}\right)^{3/2} \quad \text{Eq. S15}$$

3189 1139 Incorporating now eq. S13 into eq. S15, we can deduce:

$$3190 \quad 1140 \quad q^* = \left(\frac{\tau_s^*}{\tau_{ss}^*}\right)^{\alpha+\beta} \cdot \left(\frac{\tau_{ms}^*}{\tau_{m_{ss}}^*}\right)^\beta \cdot \left(\frac{D_{84_s}}{D_{84_{ss}}}\right)^{3/2} \quad \text{Eq. S16}$$

3197 1141 for low transport conditions. Taking into account the expression for τ_m^* (eq. S12) and assuming a
3198
3199 1142 similar bed slope for the surface and subsurface case:

$$3200 \quad 1143 \quad \frac{\tau_{ms}^*}{\tau_{m_{ss}}^*} = \left(\frac{D_{84_s}}{D_{84_{ss}}}\right) \cdot \left(\frac{D_{50_{ss}}}{D_{50_s}}\right) \quad \text{Eq. S17}$$

3205 1144 We could now introduce the idea that the armour ratio based on the D_{50} is linearly related to the
3206
3207 1145 value based on the D_{84} (see Figure 2 in the main text of the paper):

$$3208 \quad 1146 \quad \left(\frac{D_{50_s}}{D_{50_{ss}}}\right) = f \cdot \left(\frac{D_{84_s}}{D_{84_{ss}}}\right) \quad \text{Eq. S18}$$

3213 1147 Incorporating this idea into eq. S17, then:

3220
3221
3222
3223 1148
$$\frac{\tau_{m_s}^*}{\tau_{m_{ss}}^*} = f \cdot \left(\frac{D_{84_s}}{D_{84_{ss}}}\right) \cdot \left(\frac{D_{84_s}}{D_{84_{ss}}}\right)^{-1} = f$$
 Eq. S19
3224
3225

3226 1149 Now, we can simplify eq. S16 based on eq. S19:
3227
3228

3229 1150
$$q^* = f \cdot \left(\frac{\tau_s^*}{\tau_{ss}^*}\right)^{\alpha+\beta} \cdot \left(\frac{D_{84_s}}{D_{84_{ss}}}\right)^{3/2}$$
 Eq. S20
3230
3231

3232 1151 Combining eq. S20 with that for the dimensionless Shields stress based on the D_{84} (eq. S8), then:
3233
3234

3235 1152
$$q^* = f \cdot \left(\frac{D_{84_s}}{D_{84_{ss}}}\right)^{3/2-\alpha-\beta} = f \cdot \left(\frac{D_{84_s}}{D_{84_{ss}}}\right)^{-5} \rightarrow \left(\frac{D_{84_s}}{D_{84_{ss}}}\right) = \frac{1}{f} \cdot q^{*-1/5}$$
 Eq. S21
3236
3237
3238

3239 1153 at low transport conditions.
3240
3241

3242 1154 At high transport conditions (when, $\tau_{ref}^* \gg \tau_{m_s}^*$), we should combine eq. S14 with eq. S15, and
3243
3244

3245 1155 we arrive at:
3246
3247

3248 1156
$$q^* = \left(\frac{\tau_s^*}{\tau_{ss}^*}\right)^\alpha \cdot \left(\frac{D_{84_s}}{D_{84_{ss}}}\right)^{3/2}$$
 Eq. S22
3249
3250

3251 1157 Combining this expression with that for the dimensionless Shields stress:
3252
3253

3254 1158
$$q^* = \left(\frac{D_{84_s}}{D_{84_{ss}}}\right)^{3/2-\alpha} = \left(\frac{D_{84_s}}{D_{84_{ss}}}\right)^{-1} \rightarrow \left(\frac{D_{84_s}}{D_{84_{ss}}}\right) = q^{*-1}$$
 Eq. S23
3255
3256
3257

3258 1159 at full mobility conditions.
3259
3260

3260 1160 **S. 3. How did we compute the ‘bedload supply index’ for the compiled dataset?**

3262 1161 In Section 5 of the paper, we investigated and discussed whether available field measures of
3263
3264

3264 1162 bedload fluxes may explain some trends in armour ratios (D^*) in the compiled data. More
3265
3266

3266 1163 specifically, we analysed if the ‘bedload supply index’ (q^*) (at bankfull) could be correlated to
3267
3268

3268 1164 the armour ratio in the available data and how well it adjusted to eq. S22 and/or S23 (as concluded
3269
3270

3270 1165 in S. 2). According to Dietrich et al. (1989), q^* can be estimated from eq. S6. Estimating q^* from
3271
3272

3272 1166 eq. S6 needs two inputs: i. actual bedload rates (in the numerator); and ii. bedload capacities in
3273
3274

3274 1167 the denominator. In this paper, the numerator was defined from the bedload rates measured at
3275
3276
3277
3278

3279
3280
3281
3282
3283
3284
3285
3286
3287
3288
3289
3290
3291
3292
3293
3294
3295
3296
3297
3298
3299
3300
3301
3302
3303
3304
3305
3306
3307
3308
3309
3310
3311
3312
3313
3314
3315
3316
3317
3318
3319
3320
3321
3322
3323
3324
3325
3326
3327
3328
3329
3330
3331
3332
3333
3334
3335
3336
3337

1168 (close to) dominant flows for each compiled study case. Bedload rates at dominant discharges
1169 were calculated following these steps: i. for each case study we defined the best power fit relating
1170 bedload to water discharge (based on the available bedload discharge information, see Table 1 in
1171 the paper); ii. we applied the obtained regression equation to the bankfull discharge, and we
1172 computed the bedload discharge at dominant flows. Concerning the denominator q_{ss} in eq. S6, we
1173 approached channel transport capacities (for all the selected case studies) from the bedload rates
1174 estimated using Recking's formula (eqs. S10-S11), but based on subsurface GSD.
1175 The approach followed when defining q^* was obviously different in the case of flume data. As
1176 outlined in the main text of the paper, we also benefited from the results of some flume
1177 experiments that explored the role of sediment feed reductions on surface texture (Church et al.,
1178 1998; Church and Hassan, 2000; Nelson et al., 2009). Data from these flume experiments was
1179 extracted from the graphical reading of figures presented in Venditti et al. (2017). Venditti et al.
1180 (2017) estimated q^* for these flume experiments as the ratio between the bedload transport rate
1181 after the bed has adjusted to a new sediment feed divided by the transport rate for an unarmoured
1182 bed, before any feed reduction.

1183 **S. 4. How did we compute transport-stage ratios for the compiled dataset?**

1184 In Figures 8 and 10, we worked with and analysed transport stage ratios, which are defined as the
1185 ratio between Shields stresses and the critical (or reference) Shields stresses for incipient sediment
1186 motion (Wilcock et al., 2009):

$$1187 \text{Transport stage} = \frac{\tau^*}{\tau_c^*} \quad \text{Eq. S24}$$

1188 Shields stresses are calculated for the 84th percentile of GSD in this paper, since D_{84} provides a
1189 measure of the largest grains in the bed, which probably control hydraulic roughness and
1190 morphological stability (MacKenzie et al., 2018). In eq. S24 (and Figures 8 and 10 in the paper),
1191 τ_c^* is the critical Shields stress below which no sediment transport is assumed to occur. This
1192 parameter is grain-size and slope dependent (Lamb et al., 2008; Pitlick et al., 2008; Recking,
1193 2009). Here, we estimated it based on Recking (2009):

3338
3339
3340
3341
3342
3343
3344
3345
3346
3347
3348
3349
3350
3351
3352
3353
3354
3355
3356
3357
3358
3359
3360
3361
3362
3363
3364
3365
3366
3367
3368
3369
3370
3371
3372
3373
3374
3375
3376
3377
3378
3379
3380
3381
3382
3383
3384
3385
3386
3387
3388
3389
3390
3391
3392
3393
3394
3395
3396

1194 $\tau_c^* = (1.32 \cdot S + 0.037) \cdot \left(\frac{D_{84}}{D_{50}}\right)^{-0.93}$

Eq. S25